On the combined use of rain gauges and GPM IMERG satellite rainfall products for the hydrological modelling: impact assessment of the cellular automata-based methodology on the Tanaro river basin in Italy.

5 Annalina Lombardi[1,2,X], Barbara Tomassetti[1,X], Valentina Colaiuda[1,X], Ludovico Di Antonio[3], Paolo Tuccella[1,2], Mario Montopoli[6], Giovanni Ravazzani[5], Frank Silvio Marzano[1,4,†], Raffaele Lidori[1], Giulia Panegrossi[6]

[1]CETEMPS, Centre of Excellence University of L'Aquila, via Vetoio, 67100 Coppito (L'Aquila), Italy
[2]Department of Physical and Chemical Sciences, University of L'Aquila, via Vetoio, 67100 Coppito (L'Aquila) Italy
10 [3]Univ Paris Est Creteil and Université Paris Cité, CNRS, LISA, F–94010 Créteil, France
[4] Department of Information Engineering, Electronics and Telecommunications, Sapienza University of Rome, 00184 Rome, Italy
[5] Department of Civil and Environmental Engineering, Politecnico di Milano
[6] Institute of Atmospheric Sciences and Climate (ISAC), National Research Council (CNR) 00133, Rome, Italy

[X] These authors contributed equally to this work.

Correspondence to: Annalina Lombardi (annalina.lombardi@aquila.infn.it) and Barbara Tomassetti (barbara.tomassetti@aquila.infn.it)

Abstract.

The uncertainty of hydrological forecasts is strongly related to the uncertainty of the rainfall field due to the nonlinear relationship between the spatio-temporal pattern of rainfall and runoff. Rain gauges are typically considered as reference data to rebuild precipitation fields. However, due to the density and the distribution variability of the raingauge network, the rebuilding of the precipitation field can be affected by severe errors which compromise the hydrological simulation
25 output. On the other hand, retrievals obtained from remote sensing observations provide spatially resolved precipitation fields improving their representativeness. In this regard, the comparison between simulated and observed river flow discharge is crucial for assessing the effectiveness of merged precipitation data in enhancing the model's performance and its ability to realistically simulate hydrological processes. This paper aims to investigate the hydrological impact of using the merged rainfall fields from the rain gauge Italian rainfall network and the NASA Global Precipitation Measurement
30 (GPM) IMERG precipitation product. One aspect is to highlight the benefits of applying the Cellular Automata algorithm to pre-process input data in order to merge them and reconstruct an improved version of the precipitation field.

The cellular automata approach is evaluated in the Tanaro River Basin, one of the tributaries of the Po River in Italy. As this site is characterized by the coexistence of a variety of natural morphologies, from mountain to alluvial environments, as well as the presence of significant civil and industrial settlements, it makes it a suitable case study to apply the proposed

35   approach. The latter has been applied over three different flood events occurred from November to December 2014. The results confirm that the use of merged gauge-satellite data using the Cellular Automata algorithm improves the performance of the hydrological simulation, as also confirmed by the statistical analysis performed for seventeen selected quality scores.

1 Introduction

Hydrological models are important tools for flood early warning system and management of water resources under climate change conditions. The accurate estimation of precipitation and its spatial variability within a watershed is crucial for reliable discharge simulations: the relationship between the distribution of precipitation and the calculated flow discharge is not linear; therefore, the precipitation patterns strongly influence the calculation of the runoff (e.g., Goodrich et al.; 1997, Singh, 1997; Cristiano et al, 2017).

As far as the operational activity is concerned, the hydrological models are usually forced both with observed and forecasted rainfall data, and the uncertainty of hydrological forecasts is strongly related to the uncertainty of the input rain field. Therefore, forcing the hydrological models with observed precipitation data as realistic as possible is essential to reduce the hydrological simulation uncertainty related to the forecasted rainfall field.

The rain gauge data are typically used as the main source of information (Nikolopoulos et al., 2010) to produce an Areal Precipitation Estimate (hereafter APE), even if the reproduced rainfall spatial pattern can be affected by several errors. Furthermore, rain gauges, being in-situ instruments, can be considered highly accurate only over a limited area surrounding the instrument itself. Consequently, they have a reduced capability to represent the spatial distribution in highly variable precipitation fields, such as over complex terrain which are typically poorly gauged and where the orographic precipitation effects take place. Increasing the density of the network can be a way to improve the representativeness of precipitation derived from rain gauges. WMO has established standard rules in terms of the minimum density needed to build precipitation measurement networks (Sevruk, 1992; WMO, 1994; Liang et al., 2012). However, such a standard cannot be always strictly followed due to practical reasons (e.g. geomorphological characteristics, environmental conditions, and the micro-climatic variability of the considered region). Accordingly, several regional, national, and private rain gauge networks are generally not sufficiently distributed to fully satisfy the hydrological needs.

Nevertheless, the rain gauges still represent the main source of information to spatialize precipitation. The spatialization process considers the horizontal correlation structure of rain, leading to the definition of a correlation length or radius of influence through which rain gauge measurements are extended over unobserved (i.e., ungauged) surrounding areas (e. g. Duque-Gardeazábal et al., 2018). However, the raingauge radius of influence may depends on location, time, event type (eg. convective or stratiform), network density (Gandin 1970), as well as the interpolation method implemented (Xu et al., 2013; Chacon-Hurtado et al., 2017; Andiego et al., 2018), thus leading to large uncertainties in the final APE and consequently in a reduced ability to model hydrological processes.

Remote sensing observations can represent a valuable gap filling tool, complementing the above-mentioned limitations related to the APE. In particular, since satellite observations are spatially resolved, it opens to the more direct

use of Satellite-based RainFall Estimation (hereafter SRFE) (Li et al, 2021) into hydrological models. In this work, the role of APE from rain gauges and SRFE in the hydrological models is investigated. Indeed, it is well recognized that the accuracy of the results of many hydrological calculations depends on those of APE (see Nemec, 1986). The usage of SFRE for hydrological applications depends upon the type of application, the accuracy, spatial and temporal resolution as well as the latency of the estimates: different applications have different data requirements. Kidd and Levizzani (2011) demonstrated that hydrological requirements for precipitation estimates can be divided into two main categories: high and lower resolution estimates for short- and longer-lived events, respectively. Flash flood events with rapid catchment response, necessitate of a fine spatial and temporal resolution, together with timely delivery of those estimates. Fluvial flooding and water resources are characterized by relatively long lead times and therefore some requirements can be relaxed. As a matter of fact, it has been shown that SFRE's measurement uncertainties are associated to the intensity, the duration, and the scale of the event, showing an uncertainty decrease during higher rain rates, larger domains, and longer integration time: the more the precipitation tends toward deep convection regime, the more accurate the satellite estimates are (Maggioni and Massari, 2018; Maggioni and Massari, 2019). High-mountain regions are among the most challenging environments for remote-sensing-based precipitation measurements due to extreme topography and large weather and climate variability. These regions are typically characterized by a lack of in situ measurements and hit by devastating flash floods (Dinku et al., 2007; Hong et al., 2007; Kubota et al., 2009; Tian and Peters-Lidard, 2010; 2010; Hirpa et al., 2010; Yong et al., 2010; Ghulami et al., 2017; Guo et al., 2017). In this regard, satellite sensors provide global coverage and observations in regions where in situ data is unavailable or sparse. Because of this availability, the use of satellite data for hydrological applications has gained an increased interest, also given the significant activity of space-based precipitation estimation techniques in the past few decades (Guetter et al., 1996; Tsintikidis et al. 1999; Wilk et al., 2006; Hughes, 2006; Su et al., 2008; Collischonn et al.,2008; Thieming et al. 2013; Jiang and Wang, 2019; Darko et al. 2021). However, limitations associated with the use of satellite rainfall estimates for hydrological applications related mainly to the error structure of satellite rainfall estimates (McCollum et al. 2002; Gebremichael and Krajewski 2004; Hossain and Anagnostou, 2006; Ebert et al. 2007; Dinku et al. 2007; Kirstetter et al. 2013; Maggioni et al. 2011, 2014, Falck et al. 2021) and to the rainfall error propagation through the hydrological model (Nijssen and Lettenmaier 2004; Hossain and Anagnostou 2005; Hong et al. 2006; Mei et al., 2017; Solakian et al. 2020; Camici et al., 2020; Brocca et al., 2020; Camici et al., 2022; Tramblay et al. 2023) should be considered.

The error propagation of satellite rainfall through hydrological simulation is related to many factors, such as specifications of the satellite rainfall product, basin size, spatial and temporal hydrological resolution, the used hydrologic model, and geomorphological characteristics of the area (Mei et al. 2022). Dembélé et al. (2020) highlighted that although satellite products are characterized by uncertainties, their most reliable key feature is the spatial patterns representation, which is a unique and relevant source of information for distributed hydrological models. Their results demonstrate that there are

benefits in using satellite data sets when suitably integrated in a robust model parametrization scheme. Data integration was also recognized by Shi et al. (2020) to be a key point: this work suggests that hydrological simulation results using an appropriate method for precipitation merging data can provide valuable spatially distributed rainfall leading to a more rational flood flow simulation.

Several techniques to merge different data sets and reduce uncertainties in rainfall estimation are available based on physical approaches or statistical algorithms (e.g., French & Krajewski, 1994, Todini, 2001, Li and Shao, 2010). Blending of precipitation data from different sources involves a deep understanding of the source of the observations, their characteristics, and their limits.

This paper aims to achieve two main objectives: 1) validate Cellular Automata (hereafter CA) algorithm (Packard & Wolfram (1985)) to obtain a satisfactory synthesis of rain gauge data and a satellite rainfall product, focusing on small-medium scale river basins; 2) assess the possible benefits in combining the rain gauges and SFRE to overcome the limitations provided by in situ measurements alone.

The basin studied in this work is characterized by a uniformly distributed altimetry profile, with about 27% of mountain area, allowing valuable testing of satellite data. The considered area is one of the hydrological operational activity domains of forecasting severe events. The used data source is hourly rain gauge, obtained from 352 rain gauge stations into the selected domain, distributed by the Dewetra Platform (Italian Civil Protection Department and CIMA Research Foundation, 2014) and the Global Precipitation Measurement (GPM) Integrated Multi-satellite Retrievals for GPM (IMERG), half-hourly 0.1°x0.1° (roughly 10 km x10 km).

These data sources are used to generate different rainfall datasets, with mutual correction of their implicit error characteristics. To merge the data into a single rain field, CA algorithm (Packard & Wolfram (1985)) has been implemented in the CETEMPS Hydrological Model (hereafter CHyM) (Coppola et al., 2007, Verdecchia et al., 2008b) and it is then used to test hydrological response to different input rain fields. Finally, the error evaluation deals with scoring metrics in terms of comparison between simulated and observed flow discharge.

The paper is organized as follows: the geographical framework of the study area is described in section 2; in section 3 a detailed description of the field data collection is presented whereas methods are presented in section 4. Then, in section 5 the application of the proposed approach applied to three different case studies is discussed and conclusions are drawn in section 6.

2 Study area

In the Piedmont region, the northwestern part of Italy, the Tanaro River is among the main right tributaries of the Po River in terms of catchment length (276 km) and drainage basin size (8.324 km2), and with an average flow

135   discharge of 123 m3/s. The river flows eastward across northern Italy starting in proximity of the France border, Monte Saccarello (2201 m) in the Ligurian Alps (Figure 1).

According to Degiorgis et al. (2013) the river is characterized by morphological variability. Three main areas associated with very different characteristics were defined: 1) the mountain zone, with a mean slope of about 6%, deep riverbeds, and very steep catchments; 2) the mild zone, with a mean 1% slope, mildly steep catchments, and shallower

140   riverbeds; 3) the alluvial zone, with very small values of slope.

The Tanaro is the only river among the right-bank tributaries of the Po, and it has an alpine origin, although the low elevation of the Ligurian Alps and their proximity to the sea do not allow for the formation of snowpack or glaciers large enough to provide a constant source of water during the summer; moreover, the Alpine zone constitutes only part of the basin drained by the Tanaro River. For this reason, under standard seasonal conditions the flow discharge is subject

145   to great seasonal variations with a regime more typical of an Apennine stream and a maximum flow discharge that can reach 1700 m^3/s, in spring and autumn, and a very low flow rate in summer. The natural flow discharge of the Tanaro river is strongly affected by the anthropic impact due to the fragmentation of the river channels, with dams and water regulation causing diversions between basins and irrigation. Some artificial sections intersect natural branches and some of these sub-basins are used for hydropower generation. The artificial basins along the river and its tributaries are also

150   used for flood control.

The river is exposed to severe events: it has been affected by at least 136 floods in 200 years (from 1801 to 2001). The most significant of these events occurred in November 1994, when the entire river valley was damaged (Marchi et al., 1996; Luino, 2002) and the sensor at Montecastello, located at the outlet of the river recorded a maximum flow discharge peak of 4350 m^3/s (Po River Basin Authority).

155 **3 Observed Data**

Precipitation data are recorded for the 2014 period on an hourly basis. The precipitation datasets are discussed below and include gauge dataset, satellite-only dataset and the flow discharge data on selected point stations distributed along the Tanaro river basin.

3.1 Rain Gauge data.

160   It is common to attribute an area of influence on a network of rain gauges: in detail the gauge is in the center of its circular area of influence, defined as the radius of influence, R. Shi et al. (2020) suggest that the radius of influence, also considered the average distance between stations, can be computed as:

$$R = \sqrt{\frac{S}{N}} \qquad\qquad (1)$$

165

where S is the area of the smallest circle which can cover all the rain gauges and the considered basin whereas N is the number of rain gauges considered. Reasonable station coverage means that the average radius associated with the rain gauge network should be at least comparable to the value associated with the rain bandwidth. In this study, S is the area of the Tanaro basin and N is the number of rain gauges in the basin (73 in the basin): the average distance of the next

170 station is about 11 km, but the stations are not distributed regularly. As will be discussed later, different values of R are selected for the different hydrological simulations. As discussed in Sec. 2, since the Tanaro basin is divided into three territorial sectors, the average rain gauge distance is computed for each of them (see Table 1).

3.2 Satellite-based rainfall estimates

The satellite precipitation product used in this study is the Global Precipitation Measurement (GPM) Integrated

175 Multi-satellitE Retrievals for GPM (IMERG). The products provide quasi-global (60° N–60° S) precipitation estimates combining measurements from passive microwave (PMW) radiometers comprising the GPM Low Earth Orbit (LEO) satellite constellation and infrared (IR) geostationary (GEO) sensors. The IMERG product is also available in the form of post-real-time research data, i.e., IMERG Final, after monthly rain gauge analysis is received and considered (Huffman et al., 2018, O et al., 2017). Note the IMERG Final product is considered for demonstrative purposes because such product

180 is not available in near-real time and therefore it cannot be used in an operational context that require near-real-time constrains. In this study, IMERG version 5 Final (IMERG-F) Uncalibrated (UNCAL) and Calibrated (CAL, where the monthly rain gauge data are used for bias correction), half-hourly 0.1°x0.1° (roughly 10 km x10 km) rainfall rate estimates have been used. It is worth noting that in this study IMERG V05 is used while a new version (V07) is ready to be issued at the time of the publication of our study. However, the methodological value of the combination approach shown should

185 not be affected by the product version updates, although quantitative checks could merit attention in a future work.

3.3 Observed Flow Discharge data.

Flow Discharge data (m^3 s^{-1}) are used to evaluate the hydrological model output in response to different precipitation inputs. However, several issues must be considered when the evaluation of deterministic hydrological models is used, including the need to validate them with very long observed flow discharge data time series. These data

190 are not always available, especially on small seasonal streams that are usually not instrumented. Furthermore, data on artificial water management are not available. Hence, the hydrological model validation may encounter difficulties when dealing with heavily regulated basins, as it simulates the natural river flow rate without accounting for artificial facilities.

In addition, estimates of river discharge data are associated with significant uncertainties due to various conditions such as rating curve interpolation, extrapolation, unsteady flow condition, and seasonal variations in river roughness (Di
195 Baldassarre and Montanari, 2009; Di Baldassarre and Claps, 2011).

Eight stations with long time series of flow discharge, available for the year 2014, are selected for this study. The stations are distributed over the basin, as shown in Figure 1 (blue numbers) and they are representative of the different sub-basins contained in the Tanaro river basin.

4 Methodology

200 The workflow methodology is shown in Figure 2. It includes three main tasks: precipitation gridding and assimilation data, precipitation merging data and hydrological model simulations, analysis and error score metrics calculation. Different combinations of precipitation are tested as input to the hydrological model and error scores are calculated accordingly in terms of flow discharge. The proposed technique for merging different measured rainfall at different spatial scales is based on the concepts of data assimilation (Bouttier and Courtier, 1999) with particular emphasis on the
205 transformation of point data to areal data. Observed satellite and rain gauge data are gridded respecting the resolution set-up of the hydrological model: each value of rain data (satellite or gauge) is associated with a grid point i-th of coordinates (l, m) of the selected domain. Different rain scenarios are produced, using the original datasets or merged rainfall data; the hydrological model has been forced with the different rebuilt hourly rain fields to simulate flow discharges and to evaluate each scenario.

4.1 Precipitation data gridding

In hydrological modeling, precipitation data gridding is essential to accelerate numerical processing. It involves creating an initial estimate of the precipitation field at the hydrological scale, known as the Precipitation Background Field (PBF) (Coppola et al., 2007), on a regular grid. The Cressman algorithm (Cressman, 1959) is commonly used to initialize rain field grid points within the designated domain. Due to its simplicity, the Cressman method serves as a
215 practical starting point for this initialization process (Bouttier and Courtier, 1999).

The accuracy of the merged field significantly depends on the choice of kernel function, as highlighted by Li and Shao (2010). Selecting an appropriate kernel function involves defining a rain radius. The radius of influence, denoted as R, plays a crucial role in determining the smoothness of the estimated field and controlling the spread of the kernel function: a smaller R results in a more rugged estimated field with higher variance, while a larger R yields a smoother
220 surface. Thus, the selection of the radius of influence is critical in determining the overall quality and characteristics of the estimated precipitation field in hydrological modeling applications.

Based on these considerations, given a discontinuous background field, the rainfall for each grid point of the selected domain is estimated as follows:

$$P_i = \sum_j \frac{1-(r_{ij}/R)^2}{1+(r_{ij}/R)^2} P_j \tag{2}$$

225   where P_i is the estimated rain value at the *i-th* grid point, P_j are the rainfall measurements available within the radius of influence, R, and r_{ij} is the distance between rain gauge location *j* and the grid point *i*.

Selecting a suitable value for R poses the initial challenge in the estimation process. Figure 3 illustrates the area coverage by the rain gauge network when employing a radius of influence, R, equal to 5 km. Under the optimal conditions, using observed data available for every grid point in the selected domain without significant errors, employing a direct
230   merging method such as the Cressman objective analysis scheme would still result in considerable bias at the boundary (Li and Shao, 2010; Duque-Gardeazábal et al., 2018). This indicates that while a smaller value of R may mitigate bias, it would only affect a smaller area around the boundary. However, adjusting R doesn't fully address the issue of boundary bias, as the rain bandwidth tends to be large in cases where observed points are irregularly distributed. The boundary bias issue arises from the discontinuity of the background field due to field discretization, while nonparametric merging
235   methods can only generate continuous surfaces.

To overcome this issue, a double smoothing merging method is applied. It is used to reduce the boundary bias (Li and Shao, 2010; Duque-Gardeazábal et al., 2018) as better explained in the next section. Furthermore, a strategy used by the work to avoid boundary effects is to extend the spatial domain well beyond the studied basin: this strategy is useful for a better reconstruction of the precipitation field (Figure 1). Many data used, although redundant, lead to a better
240   reconstruction of the rain field. A smaller amount of this data would probably be enough, but the work uses everything that the national rainfall network has available. Future studies could lead to identifying, given their distribution, enough rain gauges outside the basin deemed useful to overcome the boundary effect.

4.2 Precipitation data interpolation and merging: Cellular Automata technique

CA technique is used in this work as a double smoothing estimation. It is a simple mathematical idealization of
245   natural systems according to Packard & Wolfram (1985), based on the behavior that every single element of a natural system can assume. In CA, natural systems are idealized as discrete sites on a lattice, with each grid point evolving based on deterministic rules and influenced by the states of neighboring cells at discrete time steps. This approach provides a structured framework for dynamic systems modelling, reflecting the intricate interplay of elements in nature.

In the hydrological model code, a CA-based algorithm has been developed and implemented. Following CA
250   theory, the input grid is conceptualized as an aggregate of Cellular Automata, where the status of each grid point represents the value of a smoothed precipitation field.

The evolution of the precipitation status in the *i-th* grid point of the lattice ($P_i^{(new)}$) is updated according to the following rule:

$$P_i^{(new)} = P_i + \alpha\left(\sum_{i=1}^{8} \beta_j(P_j - P_i)\right) \tag{3}$$

where $P_i^{(new)}$ is carried out over all 8 surrounding cells. The coefficients β_j allow to consider the different distances between the cells. As an example, for a regular equally spaced lattice, we assume the value 1 for the cells in North, East, South and West location, and the value $1/\sqrt{2}$ for the cells located in the North-East, North-West, South-East and South-West direction respect to the cell *i-th*.

The coefficient α assumes a small value, typically ranging from 0.1 to 0.9, ensuring a gentle smoothing of the original matrix. All grid points are updated synchronously, and the smoothing continues until stability is achieved, signifying minimal changes in the calculated matrix. Notably, the grid point associated with the rainfall value available in the considered database remains unaltered by the algorithm. This process enables the hydrological model to refine and stabilize the precipitation data while preserving the integrity of observed rainfall values.

Therefore, the rule in Equation 3 can be written as follows:

$$P^{t-1} = P^t + \alpha \sum_{k=1}^{8} \frac{1}{r_k} P_k^t \tag{4}$$

where r_k is the distance between the considered cell and the neighbouring grid point. The value of rainfall in the cells is serially modified (eq. 4) and the sum is computed using only the neighbouring grid points. The CA method facilitates the assimilation and spatialization of rainfall fields, proving advantageous in achieving the high resolutions required in hydrological simulations and for integrating different precipitation data sources.

In this study, to test the assimilation of satellite rainfall data in the presence of sparse gauge stations, the CA algorithm has been implemented in the hydrological model, using two different assimilation approaches: NoModular and Modular. In the NoModular approach, a high-resolution lattice is filled with both the satellite rainfall data, and the rain gauge data, used simultaneously at each time step, prioritizing the rain gauge data. To define a PBF, the approach uses an R of 10 km, which corresponds to the satellite spatial resolution, the lowest resolution to cover the whole considered domain; CA technique is then applied. In the Modular approach, a hierarchical sequence of modules is used to assimilate the different data sets, making it possible to consider the different nature of the data. Therefore, the lattice of the considered domain can be divided into as many subdomains as the data sources type. Each subdomain can be defined as a set of grid points that have at least one rainfall value in a selected radius, R, whose value depends on the density of the

available data. Three different radii of influence were selected in this study to allow for different coverage of rain gauge data compared to the satellite data.

285   Using the CA technique, this study aims at identifying how different input data settings can affect the hydrological model performance, and if merging rain gauge and satellite rainfall data improves hydrological outputs. The degree of freedom of the input data settings are: 1) the type of data sources: variation in the sources of input data, such as rain gauge data, satellite rainfall data, or a combination of both; 2) Data Merging Approach. Comparison between two merging approaches: i) NoModular, where rain gauge and satellite data are simultaneously incorporated, prioritizing rain

290   gauge data ii) Modular, which employs a hierarchical sequence of modules to assimilate different data sets independently; 3) the radius of influence, R: exploration of different values for the radius of influence, which determines the coverage area of rain gauge data before applying the CA technique and 4) Satellite Data Type: Evaluation of hydrological model performance using both Uncalibrated and Calibrated satellite rainfall data. By systematically varying these input data settings, the study aims to provide insights into their respective impacts on the hydrological model's performance. This

295   analysis will contribute to understanding the effectiveness of data assimilation techniques in improving the accuracy and reliability of hydrological simulations.

4.3 Hydrological modelling: CETEMPS Hydrological Model

The CHyM has been applied for climatological studies (Coppola et al., 2014, Sangelantoni et al., 2019), but it mainly has

300   been used as an operational tool for early warning systems (Tomassetti et al., 2005; Ferretti et al., 2019; Colaiuda et al., 2020; Lombardi et al., 2021).

CHyM is a distributed, physically based hydrological model; hydrological processes (surface runoff, infiltration, evapotranspiration, percolation, melting and return flow) are explicitly simulated. In addition to being used to acquire different data sources or rebuild the spatial distribution of precipitation at hydrological model scale, the CA algorithm

305   allows the model to simulate the hydrologic cycle of any defined geographic domain and at any fixed spatial resolution up to the Digital Elevation Model (DEM) resolution (90 meters in the current version). The choice of spatial resolution is mainly related to the validity of the numerical schemes used to simulate hydrological processes (such as the shallow water kinematic wave used to solve the continuity equation which is considered a good approximation at a horizontal resolution of a few hundred meters). The hydrological simulation spatial resolution is also related to the different simulated basins:

310   in areas with very small basins close to each other the resolution must be higher, even up to a few hundred meters; in detailed, in this work the used spatial resolution is 900m. Using ChyM, the spatial domain is extended well beyond the investigated basin. This approach is useful to avoid boundary effects and to have a better rebuild of the precipitation field. Furthermore, CHyM is a valid tool to investigate the rebuilt of the rainfall field, given that the resulting flow discharge

value is linked exclusively to the rainfall, in fact the effects related to the base flow discharge are not visible, since the model does not reproduce them, given the short simulation spin-up time. The hydrological model is not specifically calibrated over the Tarano basin. However, in this work we refer to the calibration accomplished by (Coppola at al 2014) on the northern part of the Po River, which totally includes the Tanaro basin.

4.4 Error Score Metrics

To assess the fit between the observed and simulated flow discharge time series, objective functions were selected. The traditional performance indicators have been used, such as the Nash–Sutcliffe Efficiency (NSE) (Nash and Sutcliffe, 1970), and bias percentage (PBIAS) measuring the average tendency of the simulated values to be larger or smaller than the observed ones. The optimal value of PBIAS is 0.0, with low-magnitude values indicating accurate model simulations. Furthermore, the following scores were considered: Root Mean Square Error (RMSE), Mean Absolute Relative Error (MARE), sensitive to extreme values (i.e., outliers) and to low values, Original Kling-Gupta Efficiency (KGE, Gupta et al., 2009), Modified Kling-Gupta Efficiency (KGEprime, Kingl eta al., 2012), Non-Parametric Kling-Gupta Efficiency (KGEnp, Pool et al., 2012).

According to Mathevet et al. (2006), KGE and NSE can be calculated in a bounded version: Bounded Nash-Sutcliffe Efficiency (NSEc2m), Bounded Original Kling-Gupta Efficiency (KGEc2m), Bounded Non-Parametric Kling-Gupta Efficiency (KGEmp_c2m), Bounded Modified Kling-Gupta Efficiency (KGEprime_c2m). The analysis is carried out using an open-source evaluator for flow discharge time series (Hallouin, 2019). In addition to the conventional scores, other indicators were selected to obtain a more objective analysis, independent of the limits of the scores commonly used for hydrological analyses, for a total of 17 quality scores. The idea is to consider the river flow discharge profile as a signal and for this reason, indicators, commonly used in generic signal studies, have been used.

The Match Correlation (MC) is the relationship between the Auto-correlation curve and the Cross-Correlation curve (Observed VS Simulated) and allows to understand the two curves overlap: the best value obtained will be close to 1.

$$MC = \frac{\int AutoCorrelation\_of\_Observed\_values}{\int CrossCorrelation\_of\_Index\_values\_VS\_Observed\_values} \tag{5}$$

The cross correlation (CC) is typically used in the signal theory for the assessment of similarity between two signals (Rabiner and Gold, 1975; Rabiner and Schafer, 1978; Benesty et al., 2004). The Correlation Time Delay (CT_D, Lombardi et al., 2021) represents an estimation of time shift between two series:

$$CT\_D = \max_{L \in R} CC(L) \tag{6}$$

the value of time lag L maximizes the product obtained in the CC calculation. Therefore, this quality score is suitable for measuring the effectiveness of the signal provided by hydrological simulations. The Time Peak Delay (TP_D) is a timing score and represents the hourly delay of the estimated maximum peak flow discharge compared to the observed one. The percentage Error (E%) at the peak value of the flow discharge was calculated as follows:

$$E = \frac{\max D_{Sim} - \max D_{Obs}}{\max D_{Obs}} \tag{7}$$

where D_{sim} indicates the simulated flow discharge and D_{Obs} represents the observed flow discharge.

The Dynamic Time Warping (DTW, Berndt and Clifford, 1994; Keogh and Ratanamahatana, 2005; Maier-

Gerber et al., 2019 and Di Muzio et al., 2019) finds the similarity between two sequences by looking for the best alignment. For the N-by-M matrix, built using two discrete series $x(i)$ and $y(j)$ of N and M components respectively, a "warping" path W is defined as a contiguous set of L matrix elements, and the measure of misalignment d for the path W is given by:

$$d(W) = \frac{\sum_{i,j} V(i,j)}{\frac{1}{2}L(L-1)} \tag{8}$$

where the sum in the numerator is carried out over all the elements belonging to the warping path W. Each element $V(i,j)$ represents the Euclidean distance between the i-*th* element of the first sequence and j-*th* element of the second sequence. The denominator is used to normalize different length sequences. The DTW index is then calculated as the minimum

value of $d(W)$, considering all the possible path W.

$$DTW = \min_{W} \ d(W) \tag{9}$$

The optimal path will be the N diagonal elements of matrix V, if the two considered sequences are aligned and have the

same number of components (N=M). The DTW technique, however, could lead to wrong results in finding the optimal alignment because a feature (e.g., a local peak or minimum) in one sequence is higher or lower than the corresponding feature in the other sequence. To overcome this issue, Keogh and Pazzani (2001) proposed the computation of warping using the local derivative of the time series to be compared: the Derivative Dynamic Time Warping (DDTW). The first derivative was calculated for each time series as follows:

$$D(x[i]) = \frac{(x[i]-x[i-1])+((x[i+1]-x[i-1])/2}{2} \tag{10}$$

The main limitation linked to both analyses is defined singularities (Sakoe, & Chiba 1978; Keogh and Pazzani, 2001), i.e., the algorithm may try to explain variability in the Y-axis by warping the X-axis. This can lead to unintuitive alignments where a single point on one time series maps onto a large subsection of another time series. To overcome these limits, we used the Windowing method (Berndt and Clifford, 1994). Allowable elements of the matrix can be restricted to those that fall into a warping window defined according to the following rule:

$$|i - (n/(m/j))| < \omega \tag{11}$$

where i and j are the allowable points of the nxm matrix, constrained to fall within a given warping window, ω a positive integer window width. In this work, ω is equal to 10 and this allows us to mitigate the effects linked to the baseflow discharge.

5 Analyzed case studies.

One of the effective strategies for the validation of satellite rainfall data is an indirect method through a hydrological assessment. It is worth noting that data on artificial water management are not available for the case study considered, thus, a preliminary screening is carried out to minimize any anthropogenic impact in our analysis.

In this study, the hydrological simulation ranges from November 1, 2014, to December 31, 2014. Since the purpose of this work is to investigate the performance according to the different rain scenarios (model forcing), November and December represent the most suitable period from the climatic point of view: in fact, according to the authors' experience, the succession of rainfall events in the fall reduces the anthropic impact. In late fall-early winter dams and reservoirs are often at the limit of their capacity, allowing the water to laminate, the river flow discharge to be comparable to the natural one, which is simulated by the CHyM. Three time series, related to the three different flood events, have been studied:

- Case Study 01 - 10/11/2014 00UTC – 14/11/2014 23UTC
- Case Study 02 - 15/11/2014 00UTC – 20/11/2014 23UTC
- Case Study 03 - 29/11/2014 00UTC – 03/12/2014 23UTC

Figure 4a shows the synoptic charts of the fifth generation ECMWF reanalysis (ERA5) 500 hPa geopotential height and sea level pressure (Hersbach et al. 2023), related to the first analyzed case study (12 November 2014 00UTC). The European scenario was mainly characterized by the presence of a deep depression area located in the North Atlantic and by a persistent blocking system of high-pressure on the Eastern continental sector. A trough associated to the oceanic depression was slowly moving toward Eastern Mediterranean by rotating its axis. This configuration caused instability conditions in Northern Italy, with widespread precipitation especially in the North-Western sectors, and cumulated rainfall up to 250 mm in 120 hours (10 November 00UTC – 14 November 23UTC) in the area of interest (Figure 4d).

The synoptic scenario for the second case study (16 Novmber 2014 00UTC) resulted from a slow evolution of that described above. As shown in Figure 4b, the circulation was slowed down by a high-pressure system located on Eastern Europe, extending from Anatoly up to North Sea, blocking the shift of the Oceanic trough toward the East. The most intense precipitation was registered in the Italian Northwestern sectors, with cumulated rainfall up to 250 mm in 120 hours (15 November 00UTC – 19 November 23UTC) in the area of interest (Figure 4e).

Figure 4c shows the synoptic situation related to the third case study (1 December 2014 00UTC). In this period, the typical Western Mediterranean weather conditions were affected by the evolution of a deep cut-off low. On 29 November, it was centered on Morocco and in the following days, it moved eastward, advecting subtropical warm and moist air towards northwestern Italy. The flux produced intense precipitations on the Ligurian territory, with cumulated rainfall up to 150mm in 120 hours (29 November 00UTC – 03 December 23UTC) in the area of interest (Figure 4d).

Eight different hourly simulations have been carried out for each case study, using the eight different rain input settings (Table 2). Hourly hydrological simulations are possible thanks to the availability of the observed data: the temporal resolution of the hydrological simulations, especially for small hydrological basins that have very short recharge times, is very important, given that satellite data are provided every half hour, they are essential for developing operational monitoring and forecasting tools for flood early warning systems. Therefore, UNCAL and CAL simulations use only satellite data (respectively IMERG-F Uncalibrated and IMERG-F Calibrated), while the GAUGE simulation uses the local rain gauge data; the GAUGEUNCAL simulation uses the combined gauge and satellite data using the NoModular approach. MODGAUGEUNCAL1, MODGAUGEUNCAL3, MODGAUGEUNCAL5 are the simulations where the hydrological model has been forced using a Modular approach and different radii of influence related to rain gauge data merging gauge and Uncalibrated satellite data (the number at the end of the simulation name is related to the gauge radius of influence: 1km, 3km and 5km); whereas the last hydrological simulation, MODGAUGECAL5 is carried out in the same way, but using the Calibrated satellite data.

6 Results: hydrological simulation analysis

The experiment uses an indirect validation technique of precipitation data, through an analysis of the flow discharge simulated by CHyM, where the model has been forced with eight rainfall scenarios. The APE produced using IMERG F UnCalibatred (UNCAL) and Calibrated (CAL) and rain gauge data (GAUGE) separately, is based on different R for each dataset, as defined in Equation (1). Note that in the case of satellite data, R is fixed to 10 km (the IMERG products resolution). In the case of the GAUGE, R has been set at 30km, as in the CETEMPS hydrological operational set-up (Colaiuda et al., 2020), to have a coverage of all the points of the grid in the considered domain. Therefore, even if the number of rain gauges that fall in the analyzed basin, according to equation (1), gives an average distance of the next station of about 11 km, in order to have a total coverage of the entire simulated domain (defined by the coordinates: $43.9 \leq$ latitude ≤ 46.59 and $6.49 \leq$ longitude ≤ 9.18) and to account for the rain gauge spatial distribution, R cannot be lower than 30 km.

Figure 5 shows the CHyM rebuilt rain field for the Case Study 01. In detail, Fig. 5a represents 120h accumulated rain carried out from GAUGE simulation obtained forcing the hydrological model with rain gauge data; Fig. 5b and Fig. 5c respectively represent CAL and UNCAL simulations, where CHyM has been forced using respectively GPM IMERG FINAL CAL and GPM IMERG FINAL UNCAL. Figure 5f shows the 120h cumulated rain related to MODGAUGEUNCAL5 simulation, obtained forcing the hydrological model with rain gauge data, using a Radius of influence equal to 5km, merged with GPM IMERG FINAL UNCAL.

The preliminary comparisons related to Case Study 01, between observed and simulated flow discharge data with the different rainfall scenarios are shown: in Figure 6 Alba Tanaro and Ponte di Nava sections were selected for this quick comparison. The hydrometric stations are in sections draining respectively 3385 km^2 and 145 km^2 upstream. From a first subjective analysis, the model appears to perform better with the GAUGE (cyan line), compared to the use of satellite data only, both UNCAL (gray line) and CAL (yellow line) (Figure 6 a, c), consistently with the literature: rain gauges can be considered as the most accurate approach for measurements. A sensitivity series of tests have been carried out and the most significant are reported (figure 6 b, d). The tests refer to i) the used approach: NoModular or Modular; ii) the value of R: 5 km, 3 km and 1 km for the rain gauge data and 10 km for satellite data respectively; iii) the satellite data used: GPM IMERG FINAL UNCAL and GPM IMERG FINAL CAL.

From the analysis of Figure 6, it can be deduced that the best performances are obtained for MODGAUGECAL5, although comparable performances are obtained using MODGAUGEUNCAL5 (indeed, given the small difference between the two results, the two curves are graphically superimposed). In these cases, the background rain field of the rain gauge data with $R = 5$ km (a coverage of 68% of the surface of the considered basin, Table 1), smoothed with CA, is merged with the remaining part of the surface covered by the satellite data, where its background areal is first created

with a $R = 10$ km, filling the grid points left uncovered (32%) and then applying a definitive smoothing with CA. The scores also confirm the best performances obtained by the simulation using the merged data. As an example, for the CS 01 at the ALBA section river, the KGE assumes values ranging from -1.16 (UNCAL), -0.95 (CAL), -0.703 (MODGAUGEUNCAL1), -0.366 (GAUGEUNCAL), 0.066 (GAUGE), passing to 0.209 (MODGAUGEUNCAL3), up to 0.584 (MODGAUGEUNCAL5) and 0.585 (MODGAUGECAL5).

Figure 7 shows the boxplots for KGE and RMSE related to all Case Studies and all river sections and confirms what has been shown so far: certainly, the rain gauge data allows for better performance than using the satellite data alone, but the best results are obtained when the two data sources are merged, especially using the MODGAUGECAL5 setting, which is comparable to MODGAUGEUNCAL5.

To obtain an objective evaluation, the statistical analysis has been performed using different quality scores, evaluating their overall average (AVG) related to the three Case Studies and all stations (Table 3). Table 3 is divided into two parts and the various settings have been placed following the order of increasing performance. In the first part of Table 3 an improvement corresponds to increasing values, while in the second part an improvement corresponds to decreasing values. All scores confirm the results obtained from the comparison between observed and simulated flow discharges (Figure 6), showing better performance using the rain gauge data only (GAUGE) compared to satellite data only. Simultaneously, the calibrated satellite data (CAL) allows the model to perform better than the uncalibrated ones (UNCAL). There is an evident improvement in the results obtained by merging the different sources of observed data (gauge and satellite) compared to simulations that use only satellite data.

The KGE score, for example, shows the above: an AVG ranging from -1.41 for UNCAL to 0.11 for GAUGE to 0.40 for MODGAUGECAL5 (Table 3). The MODGAUGEUNCAL3 has comparable performance, although lower, with respect to GAUGE (only rain gauge data) and to the MODGAUGEUNCAL5 and MODGAUGECAL5, where the rain gauge data have a coverage of 68%. Although they do not improve compared to GAUGE, this is encouraging, suggesting that even with a lower rain gauge density the performance of the hydrological simulation can be guaranteed. MODGAUGEUNCAL1 has been used to test the minimum bandwidth of rain gauge size in the basin. Not all results are satisfactory; for example, in the case of NSE, a classic skill score in hydrology, it is a convenient and popular (albeit gross) indicator of the model's ability (there has been a long and lively discussion about its eligibility (Gupta et al., 2009)). The simulation efficiency can be considered significant if the results are greater than 0: the study results do not respect these conditions, they are negative or at most close to zero. Although the results, our aim is to verify which APE obtained with the different settings improves the performance of the hydrological model and the results obtained with NSE test confirm it: the score goes from -15.618 for the UNCAL simulation (the worst performance) to -0.104 for MODGAUGEUNCAL5 and MODGAUGECAL5 simulations. Figure 8 shows the AVG values, listed in Table 3, of some

of the considered scores. In detail, Figure 8a shows some of the scores where the best performances are identified by a value equal to 1: KGEnp, NSEc2m, KGEc2m and MC.

In the second part of Table 3, the error is measured in terms of RMSE, MARE and PBIAS. In the case of RMSE and MARE, the trend of the results confirms what has been verified with the other quality scores. For what concerns PBIAS, the results are slightly different. The low magnitude of PBIAS indicates an accurate model simulation, positive values indicate overestimation, whereas negative values indicate model underestimation. In this case, the best performances are evident for MODGAUGEUNACAL3, GAUGE, MODGAUGEUNCAL5 and MODGAUGECAL5 simulations, although their interpretation is not as straightforward as for other scores. In detail, the overall PBIAS AVG values are 8.22 for MODGAUGEUNACAL3, -13.33 for GAUGE, and about 15 for MODGAUGEUNCAL5 and MODGAUGECAL5 simulations. Also, in this case, as shown in Table 3 and Figure 8 b CT_D, TP_D, E%, DTW, DDTW, an improvement in performance is confirmed with a clear decrease in the trend.

The comparison between the different Modular settings was necessary to verify if CA technique could overcome the limit of the satellite rain data calibration. In fact, using a 5km rain gauge radius of influence, the results are comparable both for calibrated and uncalibrated satellite data.

Regardless of the setting of the different runs, an improvement in results is obtained by merging rain gauges and uncalibrated satellite data compared to using only calibrated GPM IMERG; an improvement was also found by merging the data compared with using only rain gauge data. Thus, the Modular approach with $R = 1$ km (MODGAUGEUNCAL1) provides a lower-performing hydrological simulation than the NoModular approach (GAUNGEUNCAL), while a strong performance improvement is evident with the Modular approach, where rain gauges have $R = 5$ km (MODGAUGEUNCAL5 and MODGAUGECAL5), compared with the simulation using only rain gauge data (GAUGE). All the other scores reflect the expected trend: the performance of the model improves by merging the data, but above all, using this approach, whether calibrated or uncalibrated satellite data are used, the performances are comparable. In addition to using the average values (AVG) of the scores, the overall median (MED) and the overall standard deviation (STD) for the different runs have been computed and they are reported in the Supplementary materials (Table 4 and Table 5). A general increase in performance using merged data is obtained also for MED and for STD.

7 Conclusions

Hydrological models are crucial aids for flood early warning systems and water resource management, particularly in the context of climate change. The accuracy of the results of many hydrological calculations depends on the accuracy of the Areal Precipitation Estimation (APE): a more realistic rainfall distribution is as important as the correct estimation of the cumulative rainfall maxima, especially when severe weather events affect areas with a complex drainage

network and characterized by small to medium-sized river basins in close proximity to each other. Accurate estimation of APE using rain gauge measurement interpolation is widely used, although the use of radar and satellite data is increasingly common. To correct spatial errors caused by variability in precipitation over short distances, different data sources are necessary. As these errors are linked to the density and distribution of rain gauges, they impact the streamflow simulation model's performance. In fact, the arrangement of rain gauges in the monitoring network may not meet the minimum density standard set by the WMO, as in the selected domain, particularly in areas with diverse topography. Consequently, the use of modern remote-sensing techniques, including radar or satellite data, is indispensable in regions with scarce or non-existent rain gauges.

The study highlights the benefit of using Satellite-based RainFall Estimation precipitation products for hydrological simulations, especially in those areas where there is no homogeneous distribution of rain gauges, and it is a detailed analysis of the potential usage of the Cellular Automata based algorithm developed and implemented in the CHyM code to merge different rainfall data inputs.

This work supports the relevance and provides methodologies, for dealing with different data sources simultaneously (rain gauges and satellite rainfall estimates): different data sources are used to obtain a mutual correction of the implicit error typical of different sources. An important aspect is choosing the right methodology for using the data. The main aim of this work is to validate the CA technique as a tool for creating APE using rain gauge and satellite rainfall data. The temporal resolution of these data sources (rain gauge is provided every hour instead of satellite data every half hour) is essential for developing operational monitoring and forecasting tools for flood early warning systems.

Eight different simulations have been carried out, where the hydrological model has been forced with different CA-based APE scenarios.

For the comparison between observed and simulated flow discharge time series, objective functions were selected. The traditional performance indicators have been used: KGE, NSE and the bounded version (KGEprime, KGEnp, NSEc2m, KGEc2m, KGEprime_c2m, KGEnp_c2m). RMSE, MARE, PBIAS were also considered. In addition, the typical signal theory indicators (MC, CT_D, TP_D, E%, DTW, DDTW) were selected to obtain a more objective analysis, independent of the limits of the scores commonly used for hydrological analyses.

Three different case studies have been selected and the statistical analysis has been performed using the different quality scores, evaluating their overall average related to the three Case Studies and all station time series. The results show an improvement in the performance of hydrological simulations when satellite and rain gauge data are merged. In detailed all scores confirm the better performance using the only rain gauge data (GAUGE) compared to satellite data (UNCAL, CAL), with results ranging from negative KGE values, -1.414 and -1.425 respectively for the UNCAL and CAL simulations (as reported in Table 3) to the value 0.116 of the GAUGE simulation. Considering that in the case of the KGE score the best performances are identified by values close to 1, the best performances are associated to the model

outputs forced with APE obtained starting from a rain gauge background rain field characterized by radius of influence R = 5km (i.e., when 68% coverage of the Tanaro basin is associated to the rainfall estimated through the gauge data) and the remaining part of the area is covered by the rainfall field rebuilt using the GPM IMERG product (calibrated or uncalibrated) which has a KGE value of approximately 0.4. Less performing results than the GAUGE simulation is obtained with the other settings. Obviously, the objective of this work is not to verify the perfect performance of the hydrological model, but to demonstrate how different rainfall fields can improve hydrological simulations.

The same performances are confirmed if the typical signal theory indicators are used, where the best performances are identified by values close to zero: DDTW takes values ranging from 5.43 to 3.043 for UNCAL and CAL respectively to 0.257 for the GAUGE simulation. Also, in this case the MODGAUGEUNCAL5 and MODGAUGECAL5 simulations are comparable to each other with a value of 0.192 and perform better than the other simulations. Regarding the timing indices, CT_D and TP_D the results are comparable in all simulations. Only a few hours of shifting compared to the observed data makes the performances reliable for all simulations, regardless of the rainfall field. In any case, the CT_P confirms the best performances for the MODGAUGEUNCAL5 and MODGAUGECAL5 simulations with a score value of 0.625 compared to the worst results obtained with the UNCAL and CAL simulations with a score value of -2.75. The results for TP_D are different where the best performances are obtained with the MODGAUGEUNCAL3 simulation, with an average advance of the maximum peak of approximately two hours compared to the observed data. The same result is also obtained for the PBIAS score, measuring the average tendency of the simulated values to be larger or smaller than the observed ones, where the best average performances are obtained in the MODGAUGEUNCAL3 simulation.

In the future, this method will be tested on a larger number of case studies and different river basins, as well as on other satellite products (available at different spatial, temporal resolution and shorter latency) to investigate the advantage of the proposed approach in an operational setting for near-real time hydrological applications.

Data availability

580 All raw data can be provided by the corresponding authors upon request.

DEM data are accessibile at https://land.copernicus.eu/imagery-in-situ/eu-dem/ (last access August 2023).

The fifth generation ECMWF reanalysis (ERA5) are accessibile at https://cds.climate.copernicus.eu/cdsapp#!/dataset/reanalysis-era5-pressure-levels?tab=form (last access July 2023).

Drainage Network and boundaries basin are accessible at https://www.hydrosheds.org/ (last access August 2023).

585

Author contributions

AL, BT, VC and GP planned the work; AL, BT, LDA processed the data; AL, BT and VC analysed the results; AL and BT wrote the manuscript draft; GP, VC, FSM, GR, LDA, RL, MM, and PT reviewed and edited the manuscript.

590 **Competing interests**

The authors declare that they have no conflict of interest.

References

Andiego, G., Waseem, M., Usman, M. and Mani, N. (2018) The Influence of Rain Gauge Network Density on the Performance of a Hydrological Model. Computational Water, Energy, and Environmental Engineering, 7, 27-50.

595 https://doi.org/10.4236/cweee.2018.81002, 2018.

F. Bouttier, P. Courtier: Data assimilation concepts and methods; ECMWF lecture notes, European Centre for Medium-Range Weather Forecasts, Reading, England, 1999.

Benesty, J., Chen, J., and Huang, Y.: Time-delay estimation via linear interpolation and cross correlation, IEEE Transactions on Speech and Audio Processing, vol. 12, no. 5, 2004.

600 Berndt, J. B. and Clifford, J.: Using Dynamic Time Warping to Find Patterns in Time Series, AAAIWS'94 Proceedings of the 3rd International Conference on Knowledge Discovery, 359-370, 1994.

Brocca, L., Massari, C., Pellarin, T. et al. River flow prediction in data scarce regions: soil moisture integrated satellite rainfall products outperform rain gauge observations in West Africa. Sci Rep 10, 12517. https://doi.org/10.1038/s41598-020-69343-x, 2020.

605 Camici, S., Massari, C., Ciabatta, L., Marchesini, I., and Brocca, L.: Which rainfall score is more informative about the performance in river discharge simulation? A comprehensive assessment on 1318 basins over Europe, Hydrol. Earth Syst. Sci., 24, 4869–4885, https://doi.org/10.5194/hess-24-4869-2020, 2020.

Camici, S., Giuliani, G., Brocca, L., Massari, C., Tarpanelli, A., Farahani, H. H., Sneeuw, N., Restano, M., and Benveniste, J.: Synergy between satellite observations of soil moisture and water storage anomalies for runoff estimation,

610 Geosci. Model Dev., 15, 6935–6956, https://doi.org/10.5194/gmd-15-6935-2022, 2022

Chacon-Hurtado, J. C., Alfonso, L., & Solomatine, D.: Rainfall and streamflow sensor network design: A review of applications, classification, and a proposed framework. Hydrology and Earth System Sciences, 21, 3071– 3091. https://doi.org/10.5194/hess-2016-368, 2017.

615   Colaiuda, V., Lombardi, A., Verdecchia, M., Mazzarella, V., Ricchi, A., Ferretti, R. and Tomassetti, B.: Flood Prediction: 770 Operational Hydrological Forecast with the Cetemps Hydrological Model (CHyM), Int J Environ Sci Nat Res., 24(3): 556137, doi: 10.19080/IJESNR.2020.23.556137, 2020.

Coppola, E., Tomassetti, B., Mariotti, L., Verdecchia, M. and Visconti, G.: Cellular automata algorithms for drainage network extraction and rainfall data assimilation, Hydrological Sciences Journal, 52:3, 579-592, DOI: 10.1623/hysj.52.3.579, 2007.

620   Coppola, E., Verdecchia, M., Giorgi, F., Colaiuda, V., Tomassetti, B., Lombardi, A.,Changing hydrological conditions in the Po basin under global warming, Science of The Total Environment, Volume 493,Pages 1183-1196,ISSN 0048-9697, https://doi.org/10.1016/j.scitotenv.2014.03.003, 2014.

Dembélé, M., Hrachowitz, M., Savenije, H. H. G., and Mariéthoz, G.: Improving the predictive skill of a distributed hydrological model by calibration on spatial patterns with multiple satellite datasets, Water Resour. Res., 56,
625   e2019WR026085, https://doi.org/10.1029/2019WR026085, 2020.

Degiorgis, M., Gnecco, G., Gorni, S., Roth, G., Sanguineti, M. and Taramasso, A.C.: Flood hazard assessment via threshold binary classifiers: the case study of the Tanaro River Basin, Irrig. Drain., 62 (2), pp. 1-10, 10.1002/ird.1806, 2013.

Duque-Gardeazábal, N., Zamora, D., Rodríguez, E.: Analysis of the Kernel Bandwidth Influence in the Double Smoothing
630   Merging Algorithm to Improve Rainfall Fields in Poorly Gauged Basins; 635–626; 10.29007/2xp6; 2018.

Di Baldassarre, G. and Montanari, A.: Uncertainty in river discharge observations: a quantitative analysis, Hydrol. Earth Syst. Sci., 13, 913–921, https://doi.org/10.5194/hess-13-913-2009, 2009.

Di Baldassarre, G. and Claps, P.: A hydraulic study on the applicability of flood rating curves, Hydrology Research, 42 (1), 10–19, https://doi.org/10.2166/nh.2010.098, 2011.

635   Di Muzio, E., Riemer, M., Fink, A. H., and Maier-Gerber, M.: Assessing the predictability of Medicanes in ECMWF ensemble forecasts using an object-based approach, Quarterly Journal of the Royal Meteorological Society,145:720, 1202-1217, 2019.

Eckstein, D., Künzel, V., Schäfer, L., and Winges, M.: Global Climate Risk Index 2020, Germanwatch, available online: www.germanwatch.org/en/cri , ISBN 978-3-943704-77-8, last access: 11 June 2020, 2019.

640   Darko, S., Adjei, K.A., Gyamfi, C. et al. Evaluation of RFE Satellite Precipitation and its Use in Streamflow Simulation in Poorly Gauged Basins. Environ. Process; https://doi.org/10.1007/s40710-021-00495-2; 2021.

Dinku, T., P. Ceccato, E. Grover-Kopec, M. Lemma, S. J. Connor, and C. F. Ropelewski: Validation of satellite rainfall products over East Africa's complex topography. Int. J. Remote Sens., 28, 1503–1526, 2007.

Ebert, E. E., J. E. Janowiak, and C. Kidd: Comparison of nearreal-time precipitation estimates from satellite observations and numerical models. Bull. Amer. Meteor. Soc., 88, 47–64, 2007.

Falck, Aline S., Tomasella, Javier, Diniz, Fábio L.R., Maggioni, Viviana: Applying a precipitation error model to numerical weather predictions for probabilistic flood forecasts, Journal of Hydrology, Volume 598, 126374, ISSN 0022-1694, https://doi.org/10.1016/j.jhydrol.2021.126374, 2021.

Ferretti, R., Lombardi, A., Tomassetti, B., Sangelantoni, L., Colaiuda, V., Mazzarella, V., Maiello, I., Verdecchia, M., and Redaelli, G.: A meteorological–hydrological regional ensemble forecast for an early-warning system over small Apennine catchments in Central Italy, Hydrol. Earth Syst. Sci., 24, 3135–3156, https://doi.org/10.5194/hess-24-3135-2020, 2020.

Gebremichael, M., and W. F. Krajewski: Characterization of the temporal sampling error in space-time-averaged rainfall estimates from satellites. J. Geophys. Res., 109, D11110, doi:10.1029/2004JD004509, 2004.

Gupta, H.V., Kling, H., Yilmaz, K. K., Martinez, G. F.: Decomposition of the mean squared error and NSE performance criteria: Implications for improving hydrological modelling; Journal of Hydrology; Volume 377, Issues 1–2; Pages 80-91, ISSN 0022-1694; https://doi.org/10.1016/j.jhydrol.2009.08.003: 2009.

Hallouin, T.: HydroEval: Streamflow Simulations Evaluator (Version 0.0.3). Zenodo. https://doi.org/10.5281/zenodo.2591217, 2019.

Hersbach, H., Bell, B., Berrisford, P., Biavati, G., Horányi, A., Muñoz Sabater, J., Nicolas, J., Peubey, C., Radu, R., Rozum, I., Schepers, D., Simmons, A., Soci, C., Dee, D., Thépaut, J-N: ERA5 hourly data on single levels from 1940 to present. Copernicus Climate Change Service (C3S) Climate Data Store (CDS), DOI: 10.24381/cds.adbb2d47 (Accessed on 21-07-2023), 2023

Hong, Y., K.-L. Hsu, H. Moradkhani, and S. Sorooshian: Uncertainty quantification of satellite precipitation estimation and Monte Carlo assessment of the error propagation into hydrologic response. Water Resour. Res., 42, W08421, doi:10.1029/2005WR004398, 2006.

Hossain, F. and Anagnostou, E. N.: Numerical investigation of the impact of uncertainties in satellite rainfall estimation and land surface model parameters on simulation of soil moisture. Adv. Water Resour., 28, 1336–1350; 2005

Hossain, F. and Anagnostou, E. N.:A two-dimensional satellite rainfall error model," in IEEE Transactions on Geoscience and Remote Sensing, vol. 44, no. 6, pp. 1511-1522, doi: 10.1109/TGRS.2005.863866, 2006.

Hughes, D.A.: Comparison of satellite rainfall data with observations from gauging station networks; Journal of Hydrology, 327 (3–4), pp. 399-410, 2006.

Huffman, G.J.; Bolvin, D.; Braithwaite, D.; Hsu, K.-L.; Joyce, R.; Kidd, C.; Nelkin, E.; Sorooshian, S.; Tan, J.; Xie, P. Integrated Multi-Satellite Retrievals for GPM (IMERG) Technical Documentation; NASA/GSFC: Greenbelt, MD, USA, 2018.

Italian Civil Protection Department, CIMA Research Foundation: The Dewetra Platform: A Multi-perspective Architecture for Risk Management during Emergencies. In: Hanachi C., Bénaben F., Charoy F. (Eds.), Information Systems for Crisis Response and Management in Mediterranean Countries. ISCRAM-med 2014. Lecture Notes in Business Information Processing, Cham: Springer, pp. 165-177, 2014.

Jiang, Dejuan & Wang, Kun: The Role of Satellite-Based Remote Sensing in Improving Simulated Streamflow: A Review. Water. 11. 1615. 10.3390/w11081615, 2019.

Keogh, E. J. and Pazzani, M.: Derivative Dynamic Time Warping, Proceedings of First SIAM International Conference on Data Mining, ISBN: 978-0-89871-495-1, 2001.

Kidd, C. and Levizzani, V.: Status of satellite precipitation retrievals, Hydrol. Earth Syst. Sci., 15, 1109–1116, https://doi.org/10.5194/hess-15-1109-2011, 2011.

Keogh, E. J. and Ratanamahatana, C. A.: Exact indexing of dynamic time warping, Knowledge and Information Systems, 7(3), 358-386, doi: 10.1007/s10115-004-0154-9, 2005.

Kirstetter, Pierre-Emmanuel & Viltard, Nicolas & Gosset, M.: An error model for instantaneous satellite rainfall estimates: Evaluation of BRAIN-TMI over West Africa. Quarterly Journal of the Royal Meteorological Society. 139. 10.1002/qj.1964, 2013.

Kling, H., Fuchs, M., Paulin, M.: Runoff conditions in the upper Danube basin under an ensemble of climate change scenarios, Journal of Hydrology, Volumes 424–425, Pages 264-277, ISSN 0022-1694, https://doi.org/10.1016/j.jhydrol.2012.01.011 (https://www.sciencedirect.com/science/article/pii/S0022169412000431), 2012.

Li, M., Shao, Q.: An improved statistical approach to merge satellite rainfall estimates and raingauge data, Journal of Hydrology, Volume 385, Issues 1–4, Pages 51-64, ISSN 0022-1694, https://doi.org/10.1016/j.jhydrol.2010.01.023; 2010.

Liang, S., Xiaowen Li, Jindi Wang, Advanced Remote Sensing, Academic Press, Pages 533-556, ISBN 9780123859549, https://doi.org/10.1016/B978-0-12-385954-9.00017-4, 2012.

Lombardi, A., Colaiuda, V., Verdecchia, M., and Tomassetti, B.: User-oriented hydrological indices for early warning systems with validation using post-event surveys: flood case studies in the Central Apennine District, Hydrol. Earth Syst. Sci., 25, 1969–1992, https://doi.org/10.5194/hess-25-1969-2021, 2021.

Li, X.; Chen, Y.; Deng, X.; Zhang, Y.; Chen, L. Evaluation and Hydrological Utility of the GPM IMERG Precipitation Products over the Xinfengjiang River Reservoir Basin, China. *Remote Sens.13*, 866. https://doi.org/10.3390/rs13050866, 2021.

705   Maggioni, V., Reichle, R. H., & Anagnostou, E. N. (2011). The Effect of Satellite Rainfall Error Modeling on Soil Moisture Prediction Uncertainty, Journal of Hydrometeorology, 12(3), 413-428, 2011.

Maggioni, V., Sapiano, M. R. P., Adler, R. F., Tian, Y., & Huffman, G. J.: An Error Model for Uncertainty Quantification in High-Time-Resolution Precipitation Products, Journal of Hydrometeorology, 15(3), 1274-1292. Retrieved Feb 21, from https://journals.ametsoc.org/view/journals/hydr/15/3/jhm-d-13-0112_1.xml, 2014

710   Maggioni, V. and Massari, C.: On the performance of satellite precipitation products in riverine flood modeling: A review; Journal of Hydrology; Volume 558; Pages 214-224; ISSN 0022-1694; https://doi.org/10.1016/j.jhydrol.2018.01.039, 2018.

Maggioni, V., and Massari, C (eds.). Extreme Hydroclimatic Events and Multivariate Hazards in a Changing Environment A Remote Sensing Approach, 1st Edn. Cambridge, MA: Elsevier, Inc., 2019.

715   McCollum, J. R., W. F. Krajewski, R. R. Ferraro, and M. B. Ba: Evaluation of biases of satellite rainfall estimation algorithms over the continental United States. J. Appl. Meteor., 41, 1065–1080. 2002.

Nijssen, B., and Lettenmaier, D. P.: Effect of precipitation sampling error on simulated hydrological fluxes and states: Anticipating the Global Precipitation Measurement satellites. J. Geophys. Res., 109, D02103, doi:10.1029/2003JD003497, 2004.

720   Nikolopoulos, E. I., E. N. Anagnostou, F. Hossain, M. Gebremichael, and M. Borga: Understanding the scale relationships of uncertainty propagation of satellite rainfall through a distributed hydrologic model, J. Hydrometeorol., 11, 520–532, doi:10.1175/2009JHM1169.1, 2010.

Maier-Gerber, M., Riemer, M., Fink, A. H., Knippertz, P., Di Muzio, E., and McTaggart-Cowan, R.: Tropical transition of Hurricane Chris (2012) over the North Atlantic Ocean: a multi-scale investigation of predictability, Monthly Weather
725   Review, https://doi.org/10.1175/MWR-D-18-0188.1, 2019.

Mathevet, T. , Michel, C. , Andreassian, V., Perrin, C.: A bounded version of the Nash–Sutcliffe criterion for better model assessment on large sets of basins; V. Andréassian, A. Hall, N. Chahinian, J. Schaake (Eds.), Large Sample Basin Experiment for Hydrological Model Parameterization: Results of the Model Parameter Experiment – MOPEX, IAHS Publ, p. 567; 2006.

730   Mei, Yiwen & Anagnostou, Emmanouil & Shen, Xinyi & Nikolopoulos, Efthymios.: Decomposing the Satellite Precipitation Error Propagation through the Rainfall-Runoff Processes. Advances in Water Resources. 109. 253-266. 10.1016/j.advwatres.2017.09.012, 2017.

Mei, Y., Nikolopoulos, E. I., Anagnostou, E. N., & Borga, M. (2016). Evaluating Satellite Precipitation Error Propagation in Runoff Simulations of Mountainous Basins, Journal of Hydrometeorology, 17(5), 1407-1423. Retrieved Feb 3, from
735   https://journals.ametsoc.org/view/journals/hydr/17/5/jhm-d-15-0081_1.xml, 2022.

Nash, J.E., Sutcliffe, J.V.: River flow forecasting through conceptual modelspart I - A discussion of principles. Journal of Hydrology 10 (3), 282–290; 1970.

O, S., Foelsche, U., Kirchengast, G., Fuchsberger, J., Tan, J., and Petersen, W. A.: Evaluation of GPM IMERG Early, Late, and Final rainfall estimates using WegenerNet gauge data in southeastern Austria, Hydrol. Earth Syst. Sci., 21,
740   6559–6572, https://doi.org/10.5194/hess-21-6559-2017, 2017.

Packard, N. H. & Wolfram, S.: Two-dimensional cellular automata. J. Statist. Phys. 38, 901–946, 1985.

Po River Basin Authority, LINEE GENERALI DI ASSETTO IDROGEOLOGICO E QUADRO DEGLI INTERVENTI Bacino del Tanaro (document in Italian) http://www.adbpo.it/PAI/3%20-%20Linee%20generali%20di%20assetto%20idraulico%20e%20idrogeologico/3.3%20-
745   %20Elaborato%20Piemonte/Tanaro.pdf, last access 14 June November 2023.

Pool, S., Vis, M. and Seibert, J.: Evaluating model performance: towards a non-parametric variant of the Kling-Gupta efficiency, Hydrological Sciences Journal, 63:13-14, 1941-1953, DOI: 10.1080/02626667.2018.1552002, 2018.

Rabiner, L. R. and Gold, B.: Theory and Application of Digital Signal Processing. Englewood Cliffs, NJ: Prentice-Hall, p. 401, ISBN 0139141014, 1975.

750   Rabiner, L.R. and Schafer, R.W.: Digital Processing of Speech Signals. Signal Processing Series. Upper Saddle River, NJ: Prentice Hall., 147–148, ISBN 0132136031, 1978.

Sangelantoni L, Tomassetti B, Colaiuda V, Lombardi A, Verdecchia M, Ferretti R, Redaelli G. On the Use of Original and Bias-Corrected Climate Simulations in Regional-Scale Hydrological Scenarios in the Mediterranean Basin. Atmosphere; 10(12):799. https://doi.org/10.3390/atmos10120799, 2019.

755   Sakoe, H. & Chiba, S. (1978) Dynamic programming algorithm optimization for spoken word recognition. IEEE Trans. Acoustics, Speech, and Signal Proc., Vol. ASSP-26, 43- 49.

Saouabe, T.; El Khalki, E.M.; Saidi, M.E.M.; Najmi, A.; Hadri, A.; Rachidi, S.; Jadoud, M.; Tramblay, Y. Evaluation of the GPM-IMERG Precipitation Product for Flood Modeling in a Semi-Arid Mountainous Basin in Morocco. Water, 12, 2516, 2020.

760   Shi, H., Chen, J., Li, T., Wang, G.: A new method for estimation of spatially distributed rainfall through merging satellite observations, raingauge records, and terrain digital elevation model data; Journal of Hydro-environment Research, Volume 28, Pages 1-14; ISSN 1570-6443; https://doi.org/10.1016/j.jher.2017.10.006; 2020.

Shiffman D.: The nature of code: simulating natural systems with processing, 1st ed. The Nature of Code (CC-BY-NC 3.0); 2012.

765   Solakian, J.; Maggioni, V.; Godrej, A. Investigating the Error Propagation from Satellite-Based Input Precipitation to Output Water Quality Indicators Simulated by a Hydrologic Model. *Remote Sens.* 2020, *12*, 3728. https://doi.org/10.3390/rs12223728, 2020.

Thiemig, V., Rojas, R., Zambrano-Bigiarini, M., De Roo, A.: Hydrological evaluation of satellite-based rainfall estimates over the Volta and Baro-Akobo Basin; Journal of Hydrology; Volume 499; Pages 324-338; ISSN 0022-1694; https://doi.org/10.1016/j.jhydrol.2013.07.012; 2013.

Todini, E., Influence of Parameter Estimation Uncertainty in Kriging. Hydrology and Earth System Sciences. 5. 10.5194/hess-5-215-2001.

Tomassetti, B., Coppola, E., Verdecchia, M., and Visconti, G.: Coupling a distributed grid based hydrological model and MM5 meteorological model for flooding alert mapping, Adv. Geosci., 2, 59–63, https://doi.org/10.5194/adgeo-2-59-2005, 2005.

Sevruk, B. `Snow cover measurements and areal assessment of precipitation and soil moisture', Operational Hydrology Report, 35, Publ. 749. World Meteorological Organisation, Geneva. 91 pp., 1992.

Tramblay, Y., El Khalki, El Mahdi, Ciabatta, L., Camici, S., Hanich, L., El Mehdi Saidi, M., Ezzahouani, M., Benaabidate, L., Mahé, G. and Brocca, L. River runoff estimation with satellite rainfall in Morocco, Hydrological Sciences Journal, 68:3, 474-487, DOI: 10.1080/02626667.2023.2171295, 2023.

Xu, H., Xu, C. Y., Chen, H., Zhang, Z., and Li, L.: Assessing theinfluence of rain gauge density and distribution on hydrologicalmodel performance in a humid region of China, J. Hydrol., 505,1–12, 2013.

WMO Guide to Hydrological Practices, fifth edn. WMO no. 168, World Meteorological Organization, Geneva, Switzerland, 1994.

785
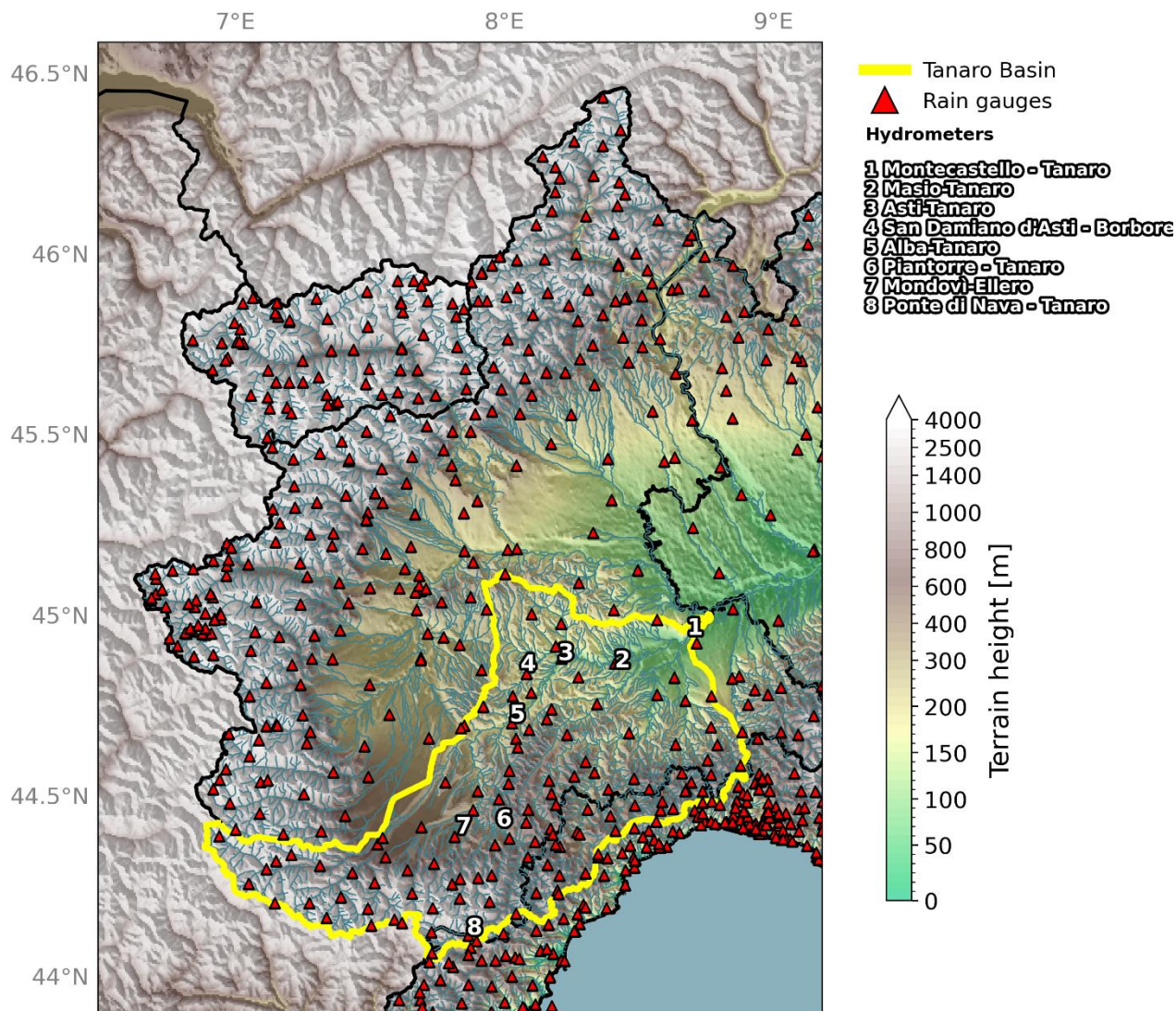
Figure 1: North-West domain of Italy main drainage network (blue line), Tanaro river basin is hilighted in yellow. The numbers represent the basin flow discharge stations selected: Montecastello (7956 km^2 drained), Masio (4535 km^2 drained), Asti (4123 km^2 drained), Alba (3385 km^2 drained), Piantorre (500 km^2 drained), Mondovì – Ellero (180 km^2 drained), San Damiano d'Asti – Borbore (85 km^2 drained), Ponte di Nava (149 km^2 drained). The red triangles are the rain gauges available for this study. DEM data are accessibile at https://land.copernicus.eu/imagery-in-situ/eu-dem/ (last access August 2023). Drainage Network and boundaries basin are accessible at https://www.hydrosheds.org/ (last access August 2023).

795
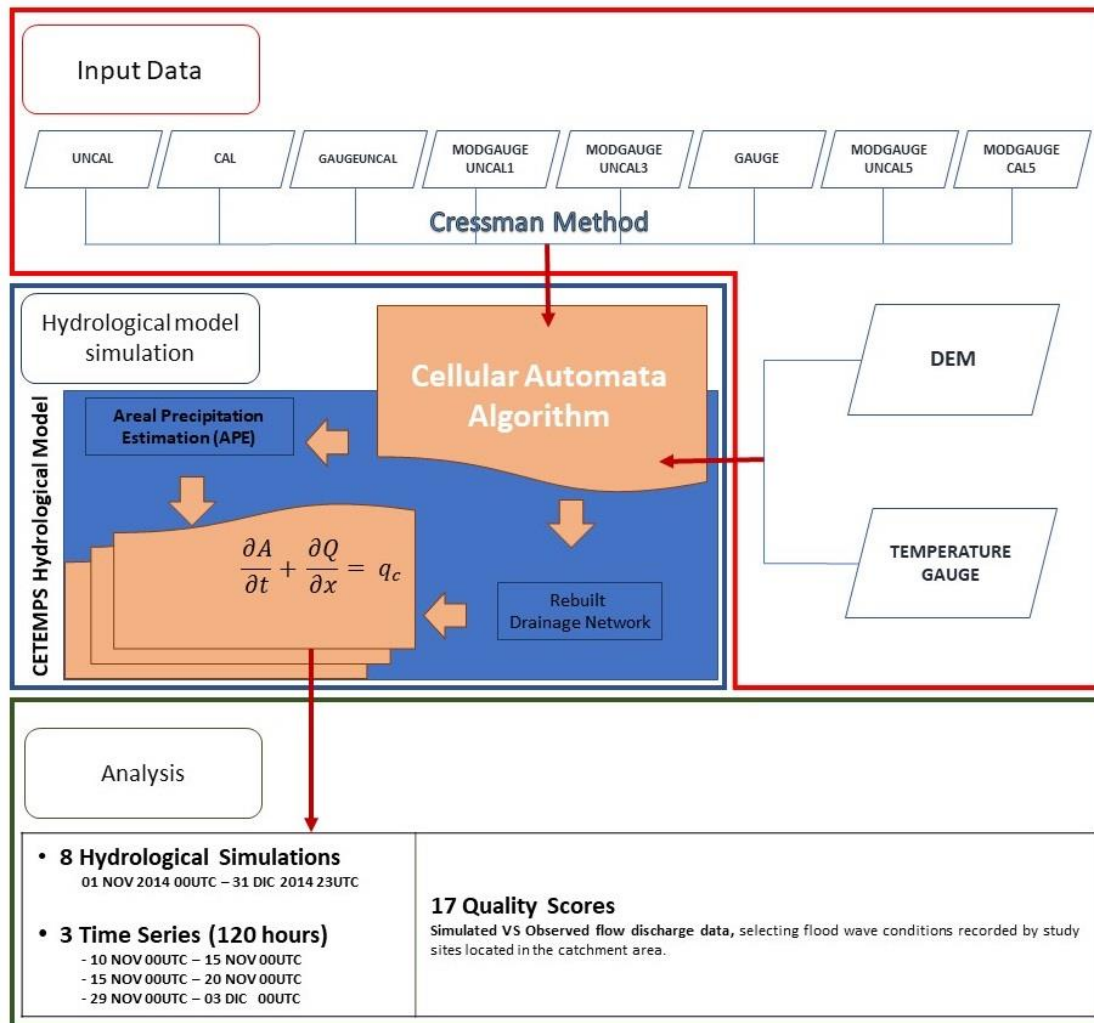
Figure 2. Numerical experiment workflow, consisting of three main tasks: 1) precipitation gridding and assimilation data, 2) precipitation merging data and hydrological model simulations, 3) analysis and error score calculation. Different combinations of precipitation are tested as input to the hydrological model and error scores calculated accordingly in terms of flow discharge. Eight different simulations have been carried out for each case studies, using the eight different rain input settings.

800
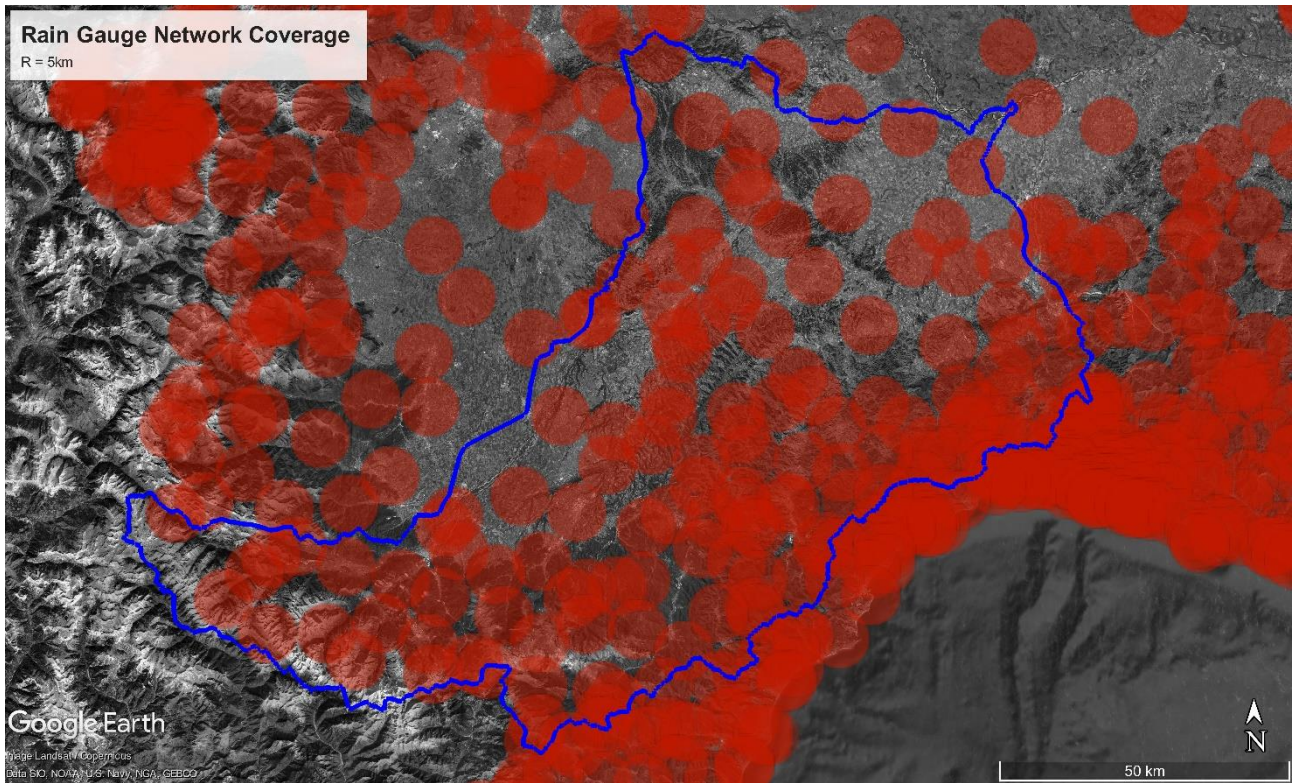
Figure 3. Tanaro Basin rain gauge density and distribution. The red circles represents the rain gauge coverage of area using a radius of influence of 5 km. The blue line reprents the Tanaro basin extent. @Google Earth.
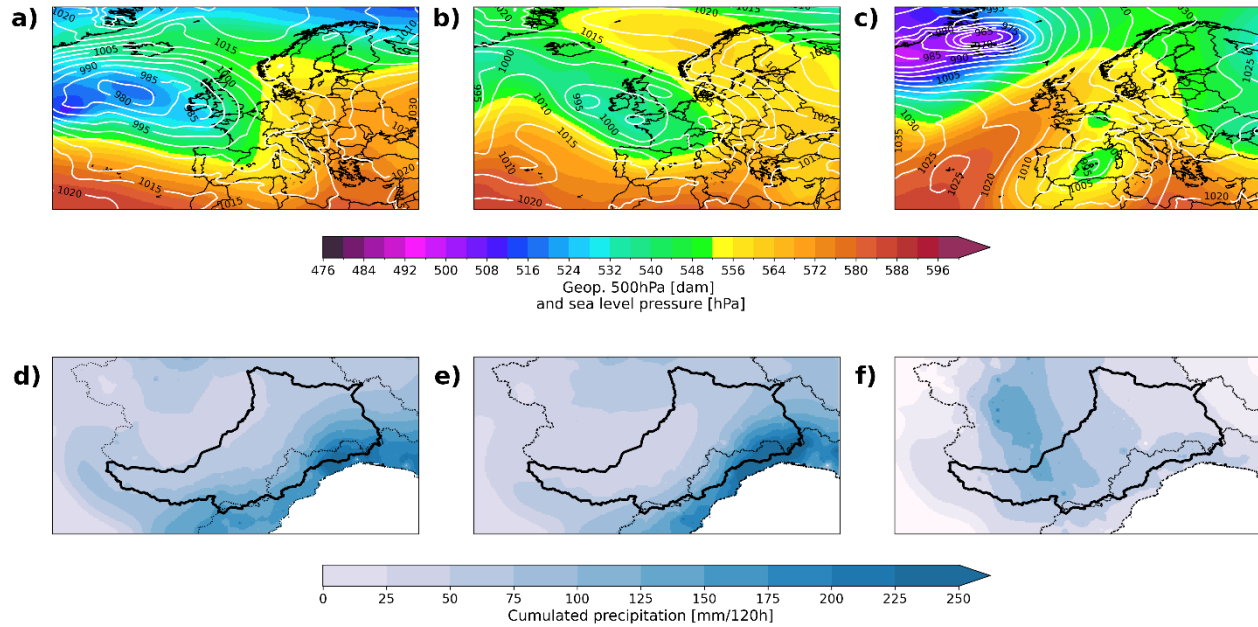
Figure 4. Case Studies Synoptic analysis: a) CS 01 12 November 2014 00UTC, b) CS 02 16 November 2014 00UTC, c) CS 03(1 December 2014 00UTC) 500 hPa geopotential height and sea level pressure using the fifth generation ECMWF reanalysis (ERA5); d) CS 01, e) CS 02, f) CS 03 120h cumulated rain rebuilt using rain gauge data.
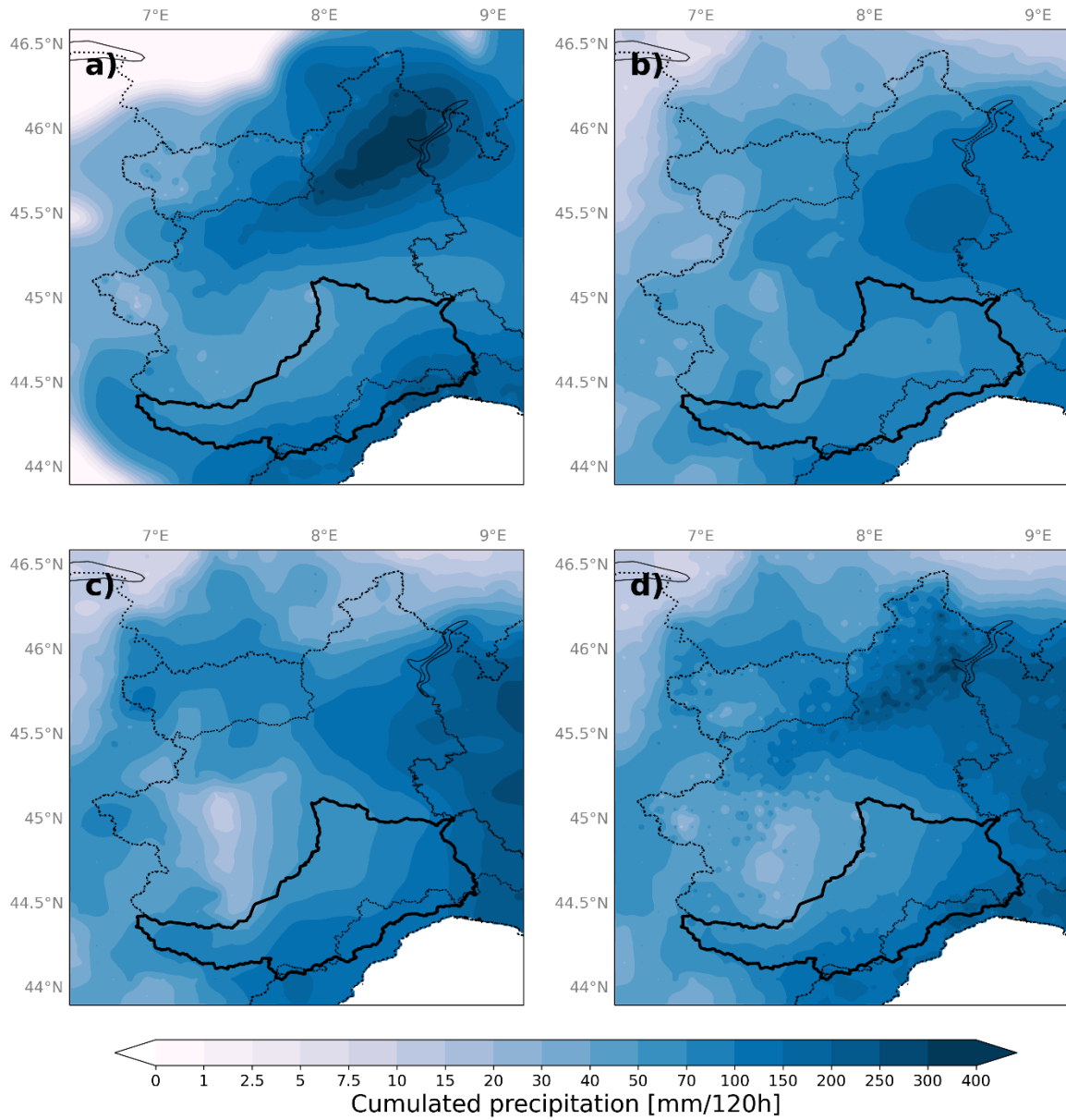
Figure 5: CS 01 Areal Precipitation Estimation: the figures show the rain field rebuilt using rain gauge data (a), GPM IMERG FINAL CAL (b), GPM IMERG FINAL UNCAL (c). Panel d shows the rain field obtained forcing the hydrological model with rain gauge data, using a radius of influence equal to 5km, merged with GPM IMERG FINAL UNCAL.

820
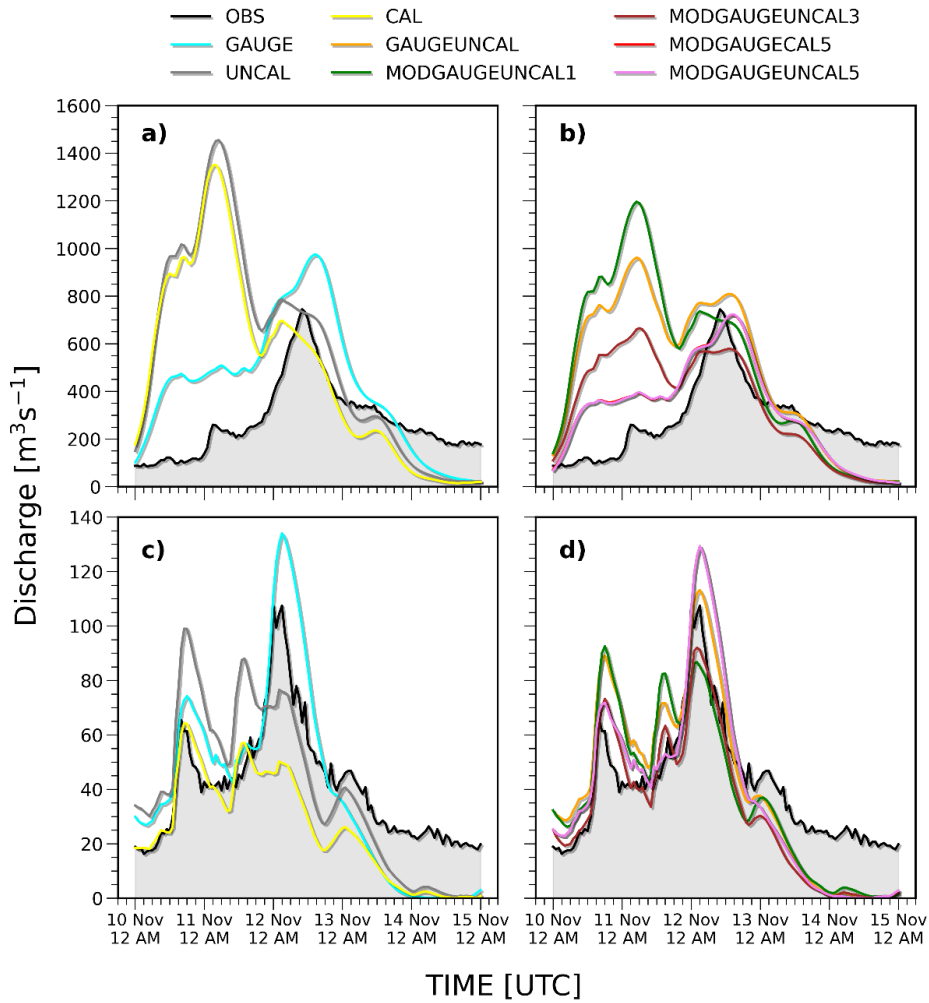
Figure. 6. Intercomparison between Observed and Simulated flow discharge data with the different rainfall scenarios for CS01. The Simulation analysis are related to Alba Tanaro (a, b) and Ponte di Nava (c, d) river sections.

825
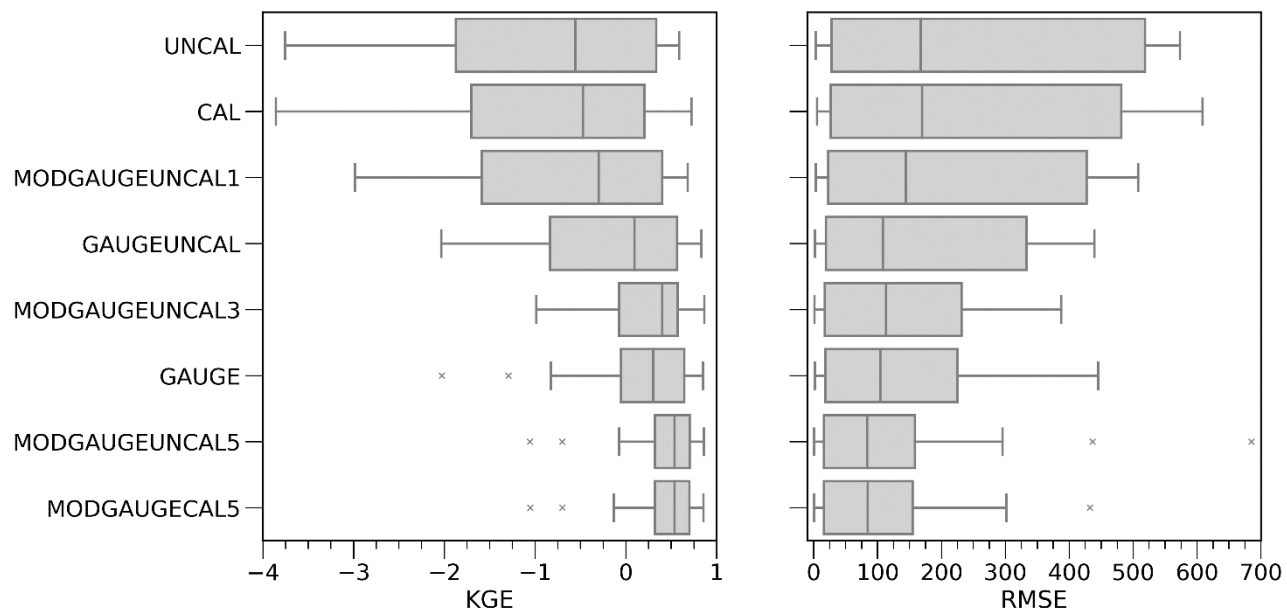
Figure 7. The boxplots show the summary refer to KGE and RMSE obtained from the CHYM simulation using the eight APE fields as input, related to all three Case Studies and all river sections.
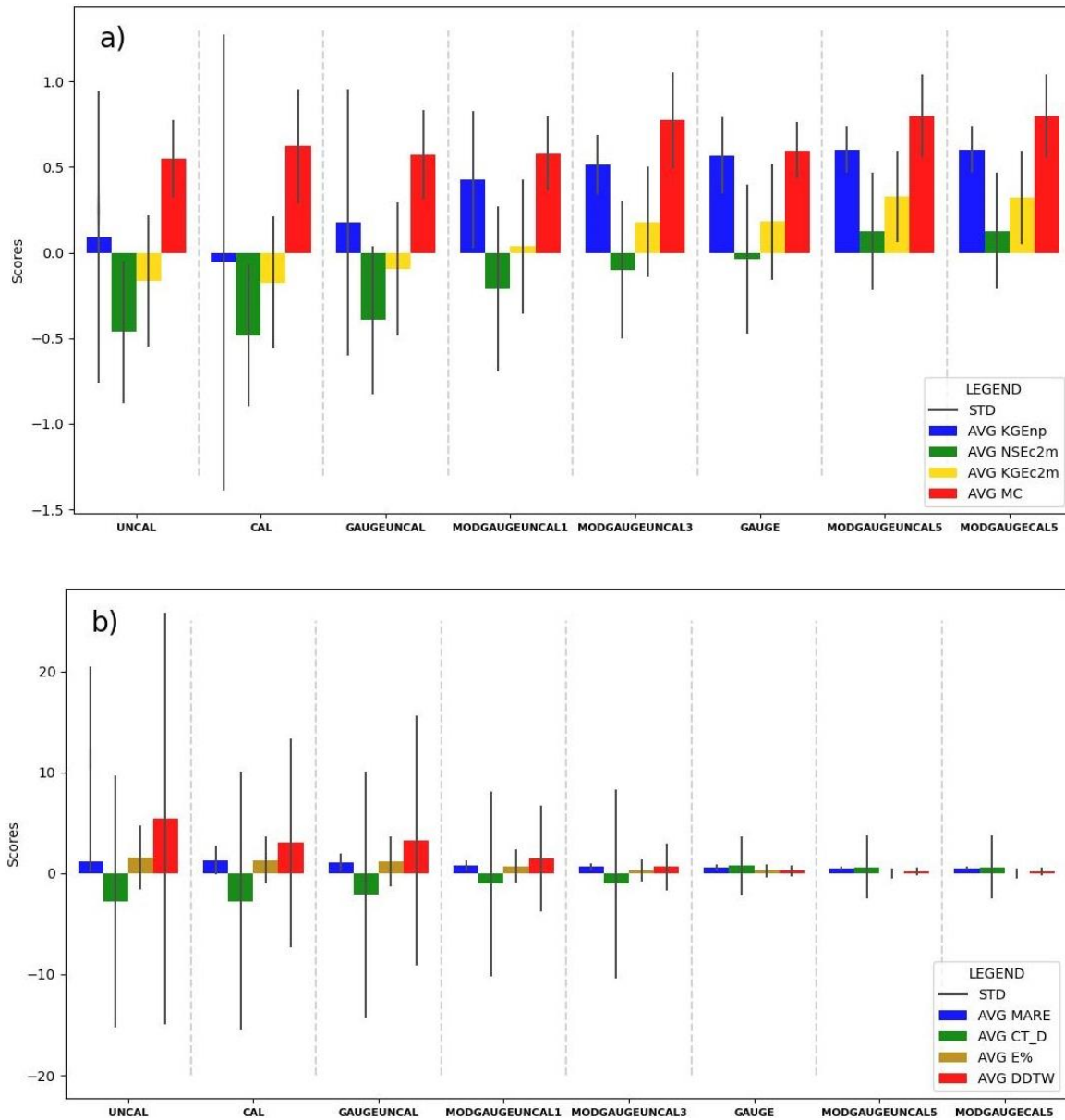
Figure 8. The histograms summarize the statistical analysis performed for the different scores, evaluating their average (AVG) and the standard deviation (STD). The figure a) shows the quality scores (KGEnp, NSEc2m, KGEc2m and MC) where the best performances are identified by a value equal to 1. In the figure b) (MARE, CT_D, E% and DDTW) the best performances are identified by values close to zero.

Table 1. Raingauge Network characteristic of Tanaro catchment; R[*] = Cressman radius of influence.

Region Type	Area size (km²)	Network characteristics		Average Gauge Distance (km)	Gauge Covered Area (R=5km) *	Gauge Covered Area (R=3km) *	Gauge Covered Area (R=1km) *
		Gauge Numbers	Network Density (km² per gauge)				
Mountain (>700 MSL)	2241	22	102	10	0.79	0.26	0.006
Hill (700 ≤ H ≤ 300)	3032	32	95	9.74	0.74	0.26	0.008
Flat (< 300)	3153	19	166	13	0.51	0.16	0.004
Tanaro Catchment	**8426**	**73**	**115**	**10.74**	**0.68**	**0.22**	**0.006**

840

Table 2. Input data sources and settings for each simulation.

Simulation	Input data souces	Radius of influence
UNCAL	IMERG F Uncal	10 km
CAL	IMERG F Cal	10 km
GAUGE	Rain Gauge	30 km
GAUGEUNCAL (NoModular)	Rain Gauge + IMERG F Uncal	10 km
MODGAUGEUNCAL1	Rain Gauge	1 km
	IMERG F Uncal	10 km
MODGAUGEUNCAL3	Rain Gauge	3 km
	IMERG F Uncal	10 km
MODGAUGEUNCAL5	Rain Gauge	5 km
	IMERG F Uncal	10 km
MODGAUGECAL5	Rain Gauge	5 km
	IMERG F Cal	10 km

845

Table 3. Average statistical scores for all three case studies and all river stations obtained from the CHYM simulations using the eight APE fields as input (AVG). The first block of the table shows all the quality scores where the best performances are identified by a value equal to 1. In the second block of the table, the best performances are identified by values close to zero.

	UNCAL	CAL	MOD GAUGE UNCAL1	GAUGE UNCAL	MOD GAUGE UNCAL3	GAUGE	MOD GAUGE UNCAL5	MOD GAUGE CAL5
KGE	-1.414	-1.425	-1.029	-0.408	0.069	0.116	0.407	0.403
NSE	-15.618	-12.739	-10.425	-4.570	-1.775	-0.997	-0.104	-0.104
KGEprime	-0.711	-0.989	-0.565	-0.139	-0.070	0.186	0.242	0.239
KGEnp	0.090	-0.056	0.178	0.427	0.514	0.568	0.604	0.604
NSEc2m	-0.462	-0.482	-0.392	-0.210	-0.101	-0.037	0.126	0.128
KGEc2m	-0.164	-0.175	-0.097	0.036	0.179	0.181	0.327	0.325
KGEprime_c2m	-0.150	-0.199	-0.112	0.034	0.069	0.202	0.251	0.250
KGEnp_c2m	0.173	0.156	0.218	0.336	0.363	0.428	0.446	0.447
MC	0.548	0.622	0.572	0.579	0.774	0.598	0.798	0.797
RMSE	297.038	277.595	257.797	200.080	159.440	149.397	128.757	129.549
MARE	1.163	1.299	1.055	0.778	0.630	0.586	0.464	0.464
PBIAS	-53.840	-57.306	-43.956	-25.297	8.220	-13.323	15.662	15.383
CT_D	-2.750	-2.750	-2.125	-1.042	-1.042	0.750	0.625	0.625
TP_D	-4.083	-4.833	-3.375	-1.958	-1.875	3.875	3.750	3.792
E%	1.543	1.318	1.176	0.716	0.261	0.275	-0.021	-0.019
DTW	50.829	40.878	33.380	15.190	6.978	4.346	2.674	2.660
DDTW	5.436	3.043	3.274	1.481	0.668	0.257	0.192	0.192

Table 4. Standard deviation of the statistical scores for all three case studies and all river stations obtained from the CHYM simulations using the eight APE fields as input (STD).

	UNCAL	CAL	MOD GAUGE UNCAL1	GAUGE UNCAL	MOD GAUGE UNCAL3	GAUGE	MOD GAUGE UNCAL5	MOD GAUGE CAL5
KGE	2.914	2.617	2.386	1.536	1.003	0.701	0.445	0.448
NSE	42.912	25.613	28.062	12.344	5.752	2.480	1.226	1.228
KGEprime	1.126	1.439	1.029	0.795	0.802	0.609	0.634	0.637
KGEnp	0.854	1.333	0.779	0.402	0.173	0.224	0.138	0.137
NSEc2m	0.414	0.415	0.433	0.482	0.401	0.435	0.340	0.341
KGEc2m	0.383	0.387	0.388	0.392	0.321	0.342	0.268	0.272
KGEprime_c2m	0.298	0.315	0.298	0.298	0.297	0.316	0.332	0.333
KGEnp_c2m	0.313	0.327	0.306	0.261	0.153	0.200	0.143	0.142
MC	0.266	0.335	0.260	0.217	0.282	0.166	0.242	0.243
RMSE	366.182	289.936	324.530	244.503	191.808	167.846	159.119	164.644
MARE	0.984	1.437	0.898	0.521	0.318	0.306	0.186	0.187
PBIAS	101.932	151.940	94.248	53.677	34.796	34.535	23.365	23.417
CT_D	12.477	12.804	12.221	9.154	9.370	2.933	3.080	3.107
TP_D	14.180	14.020	14.041	12.614	12.204	3.756	3.711	3.730
E%	3.166	2.295	2.451	1.650	1.101	0.640	0.533	0.533
DTW	126.770	70.688	81.781	34.897	15.763	6.349	3.024	3.020
DDTW	20.408	10.338	12.362	5.263	2.326	0.562	0.371	0.372

870 **Table 5**. Median of the statistical scores for all three case studies and all river stations obtained from the CHYM simulations using the eight APE fields as input (MED).

	UNCAL	CAL	MOD GAUGE UNCAL1	GAUGE UNCAL	MOD GAUGE UNCAL3	GAUGE	MOD GAUGE UNCAL5	MOD GAUGE CAL5
KGE	-0.558	-0.473	-0.299	0.097	0.402	0.299	0.537	0.537
NSE	-3.140	-3.609	-2.083	-0.637	-0.264	0.046	0.341	0.331
KGEprime	-0.485	-0.585	-0.308	0.030	0.116	0.362	0.532	0.529
KGEnp	0.392	0.375	0.500	0.606	0.523	0.657	0.611	0.619
NSEc2m	-0.604	-0.643	-0.508	-0.240	-0.116	0.028	0.207	0.199
KGEc2m	-0.218	-0.182	-0.129	0.051	0.251	0.176	0.368	0.367
KGEprime_c2m	-0.195	-0.225	-0.133	0.015	0.062	0.221	0.362	0.360
KGEnp_c2m	0.244	0.231	0.333	0.435	0.354	0.489	0.440	0.448
RMSE	167.351	169.794	144.205	108.312	113.309	104.219	83.801	84.676
MARE	0.915	0.845	0.817	0.635	0.531	0.533	0.457	0.467
PBIAS	-30.560	-20.430	-17.750	-4.952	20.578	-1.279	20.597	21.030
CT_D	0.535	0.560	0.570	0.585	0.765	0.570	0.750	0.750
TP_D	2.000	1.000	1.500	1.000	1.000	0.000	0.500	0.500
E%	0.100	0.500	1.100	2.200	2.100	4.000	3.500	3.500
DTW	0.630	0.605	0.605	0.230	-0.075	0.075	-0.220	-0.220
DDTW	9.940	11.605	7.000	2.255	3.020	1.945	2.000	2.005
RMSE	0.140	0.145	0.125	0.065	0.045	0.040	0.040	0.040

875